



**Facultad
de
Ciencias**

**ON THE RADIATIVE AND NON-RADIATIVE
CONTRIBUTION TO THE ELECTROMAGNETIC
LIGHT SCATTERING BY MAGNETODIELECTRIC
PARTICLES**

**Trabajo de Fin de Grado
para acceder al**

GRADO EN FÍSICA

Autor: Yael Gutiérrez Vela

Director: Fernando Moreno Gracia

Co-Director: Francisco González Fernández

Septiembre - 2014

ABSTRACT

The angular spectrum representation of electromagnetic fields scattered by metallic particles much smaller than the incident wavelength was used to interpret and analyze the spectral response of localized surface plasmon resonances (LSPs) both in the near-field and far-zone regimes. The previously observed spectral redshift and broadening of the LSP peak, as one moves from the far-zone to the near-field region of the scatterer, was analyzed on studying the role and contribution of the evanescent and propagating plane wave components of the emitted field. For such dipolar particles, it was found that the evanescent waves are responsible for those broadenings and shifts. Further, we proved that the shift is a universal phenomenon, and hence, it constitutes a general law, its value increasing as the imaginary part of the nanostructure permittivity grows. Following these lines, and because of the recent interest on the light scattering by magnetodielectric particles, the purpose of the work we propose is investigating the physical effects of the contribution of the evanescent channel to the electromagnetic behavior of the scattered fields in the near- and far-field regimes by these particles which in turn show coherent effects between the excited dipolar electric and magnetic modes. Our results should be of use for the prediction and interpretation of the spectral behavior in applications assisting surface-enhanced Raman spectroscopy or equivalent processes with the recent proposed configurations made of dielectric nanoantennas where ohmic losses are very low.

Key words: magnetodielectric, radiative, non radiative, evanescent waves, redshift, broadening, near field, far field.

La representación angular del campo electromagnético difundido por partículas metálicas de tamaño mucho menor que la longitud de onda del campo incidente ha sido usada para interpretar y analizar la respuesta espectral de las resonancias de plasmones superficiales localizados (LSPs), tanto en campo cercano como lejano. El corrimiento al rojo y el ensanchamiento de los picos de las resonancias de los LSP cuando pasamos del campo cercano al lejano ha sido analizado mediante el estudio de la contribución de las ondas evanescentes y propagantes al campo emitido. Para este tipo de partículas dipolares, se ha observado que las ondas evanescentes son las responsables del este corrimiento al rojo y ensanchamiento. Es más, se ha probado que este corrimiento es un fenómeno universal, y por lo tanto, sirve para enunciar una nueva ley general: este corrimiento es mayor cuanto más grande es la parte imaginaria de la permitividad eléctrica de la nanoestructura. A partir de esto, y teniendo en cuenta el interés reciente en la difusión de luz por partículas magnetodieléctricas, el propósito de este trabajo es la investigación del efecto de la contribución de las ondas evanescentes al comportamiento del campo difundido en campo cercano y lejano por este tipo de partículas, las cuales muestran efectos coherentes entre los modos dipolares eléctricos y magnéticos excitados. Los resultados obtenidos deben ser útiles para la predicción e interpretación del comportamiento espectral en aplicaciones como SERS o procesos equivalentes con configuraciones propuestas hechas de nano antenas dieléctricas donde las pérdidas óhmicas son muy bajas.

Palabras clave: magnetodieléctrico, radiativo, no radiativo, ondas evanescentes, corrimiento al rojo, ensanchamiento, campo cercano, campo lejano.

INDEX

<i>1. INTRODUCTION</i>	<i>4</i>
<i>2. OBJECTIVES AND WORK SCHEME</i>	<i>6</i>
<i>2.1 OBJECTIVES</i>	<i>6</i>
<i>2.2 WORK SCHEME</i>	<i>6</i>
<i>3. THEORETICAL BACKGROUND</i>	<i>7</i>
<i>3.1 MIE'S THEORY</i>	<i>7</i>
<i>3.2 DIPOLE APPROXIMATION FOR METALLIC AND HIGH REFRACTIVE INDEX NANOPARTICLES</i>	<i>10</i>
<i>3.3 RADIATIVE AND NON RADIATIVE CONTRIBUTION</i>	<i>12</i>
<i>3.4 SPECTRAL BEHAVIOR OF LOCALIZED PLASMON RESONANCES IN NEAR AND FAR FIELD FOR METALLIC NANOPARTICLES.</i>	<i>15</i>
<i>3.5 KERKER'S CONDITIONS</i>	<i>17</i>
<i>4. RESULTS</i>	<i>18</i>
<i>4.1 LABORATORY SYSTEM</i>	<i>18</i>
<i>4.2 COMPUTER PROGRAMS</i>	<i>19</i>
<i>4.3 COMPARISON BETWEEN MIE THEORY AND THE DIPOLE APPROXIMATION</i>	<i>23</i>
<i>4.3.1 METALLIC NANOPARTICLES</i>	<i>23</i>
<i>4.3.2 HIGH REFRACTIVE INDEX NANOPARTICLES</i>	<i>24</i>
<i>4.4 SPECTRAL BEHAVIOR OF THE DIPOLE RESONANCES OF HRI NANOPARTICLES IN NEAR AND FAR FIELD.</i>	<i>26</i>
<i>4.4.1 SPECTRAL EVOLUTION OF THE ELECTRIC SCATTERED FIELD IN NEAR AND FAR FIELD.</i>	<i>26</i>
<i>4.4.2 SPECTRAL EVOLUTION OF THE MAGNETIC SCATTERED FIELD IN NEAR AND FAR FIELD.</i>	<i>27</i>
<i>4.4.4 RADIATIVE AND NON RADIATIVE CONTRIBUTION TO THE MAGNETIC FIELD SCATTERED BY HIGH REFRACTIVE INDEX NANOPARTICLES IN NEAR FIELD.</i>	<i>32</i>
<i>4.4.5 SPECTRAL EVOLUTION OF THE POYNTING VECTOR OF THE ELECTROMAGNETIC SCATTERED FIELD BY HIGH REFRACTIVE INDEX NANOPARTICLES IN FIELD IN NEAR AND FAR FIELD.</i>	<i>36</i>
<i>4.4.6 RADIATIVE AND NON RADIATIVE CONTRIBUTION TO THE POYNTING VECTOR OF THE ELECTROMAGNETIC FIELD SCATTERED BY HIGH REFRACTIVE INDEX NANOPARTICLES IN NEAR FIELD.</i>	<i>37</i>
<i>5. CONCLUSIONS</i>	<i>40</i>
<i>6. FURTHER WORK</i>	<i>41</i>
<i>7. BIBLIOGRAPHY</i>	<i>42</i>
<i>ANNEX I: WORK AT BROWN UNIVERSITY</i>	<i>43</i>

1. INTRODUCTION

Nowadays we are living in the era of the miniaturization. When Richard Feynman first postulated the possibility of direct manipulations of a bulk of atoms, or atoms themselves, in his lecture “There’s plenty of Room at the Bottom”, he set the bases of nanotechnology. What he proposed sounded futuristic and the road to that goal seemed extremely long. However, the increasing demand of miniaturized devices in fields such as medicine or communication has led to an astonishing evolution of nanotechnology.

Nanotechnology is a new branch in science in charge of the study and the manipulation of matter at a nanoscale level. When the interaction between matter and light is considered at dimensions of the nanometer we are talking about nanophotonics. One of the most important discipline in this area of study is nanoplasmonics due to its enormous quantity of applications.

Nanoplasmonics [1] studies the optical phenomena in the nanoscale vicinity of metallic surfaces. In a metallic nanoparticle electrons in the conduction band can be considered to move freely through the surface. When a metallic nanoparticle is placed in an electromagnetic field whose wavelength, λ , is bigger than its size, the free charges start to oscillate. There is a characteristic frequency which depends on the electron density of the metal known as plasma frequency. When the incident electromagnetic field oscillates with a frequency equal to the plasma frequency a resonance is produced. As a result, a charge displacement with respect to the lattice ions is produced and a *localized surface plasmon* (LSP) is created. These surface plasmons produced very intense and localized electromagnetic fields confined in the vicinity of the metallic nanoparticle surface at dimensions smaller than the wavelength.

These particular characteristics of metallic nanoparticles are used for new techniques of spectroscopy such as Surface Enhancement Raman Spectroscopy (SERS). This type of spectroscopy requires the control of the peak position of the resonance in the near field because in this region is where the molecules are placed. This position, that depends on the size and refractive index of the nanoparticle, has led to a great development in the LSP studies.

In the last years the position of the resonance peaks were calculated in terms of the scattering and extinction spectra. These types of spectra are measured at distances much larger than the wavelength, in the region known as far field. However, what is interesting for SERS is the position of the resonance peaks near the surface of the nanoparticle, at the near field regime.

More precisely, the far field is defined as the region where $kr \gg 1$, and the near field where $kr < 1$. k is a magnitude known as wavelength number and it is defined by $k = 2\pi/\lambda$. r is the distance at which the measurement is done.

One of the first experimental attempts to show the different behavior at the near and far field regimens were made by Alonso-González et al [2]. Their results showed that the resonance peak in the near field regime was red shifted with respect to the far field regime.

The explanation of this phenomenon has led to great discussion. There are interpretations based in different principles.

On the one hand, this phenomena has been explained by considering the metallic nanoparticles to behave like an electric dipole. This electric dipole was considered as a driven, damped harmonic oscillator [3, 4, 5]. This damping caused by the emission of light into the free space has been said to be the reason of the redshift.

On the other hand, this redshift has been explained in terms of the radiative and non radiative contribution to the total scattered field [6] while considering the metallic nanoparticle as an electric dipole. Whereas in far field the radiative contribution takes the lead roll and the non radiative is negligible, in near field it is the other way round.

As it has been said, depending on the particle parameters such as refractive index or size this localized surface plasmons will appear for different wavelengths. In addition, depending on the relation between the size of the particle and the wavelength of the incoming electromagnetic field the charge distribution in the surface will be more or less complex. For example, if the size of the particles is much more smaller than the wavelength of the incoming electromagnetic field, a dipolar charge distribution will appear. However, if the the size of the particle is increased, the charges in the interior of the nanoparticles are subjected to different electromagnetic fields. This anisotropy leads to more complex charge distributions and to higher order resonances such as the quadrupolar, octupolar, etc.

Although all these studies have only been done with metals, these materials present absorption, so part of the incident energy is lost by Joule effect. For this reason in the last years dielectric particles with high refractive index have become a new topic of research.

Dielectric particles with high refractive index also show this plasmonic-like resonances for certain size, configurations and incident wavelengths. Due to the fact that they do not absorb any of the radiation they have become a revolution in nowadays technology [14,15].

Dielectric materials do not have free electrons unlike metals. As a result of this difference the resonances that show high refractive index (HRI) materials, are not produced by plasmonic mechanisms as in the case of metals. However, a similar phenomenon, known as Whispering Gallery Modes, takes place.

This name was inspired in the whispering gallery of St Paul's Cathedral in London in which a whisper emitted in one point of the gallery could be heard across the dome, but not in any intermediate point. The first one who gave an explanation to this phenomena was Lord Rayleigh. The *Whispering Gallery Modes* [7] are resonances produced inside the dome. They are waves that travel around the cavity supported by continuous reflection that meet the resonance condition after each lap. As a result it interfere constructively with itself.

A similar phenomena is produced in HRI particles but instead of sound, light is the wave bouncing in the interior of the particle. Because the dielectric sphere has a refractive index higher than the medium in which it is placed, the beam suffers total reflection in the boundary between the two media. As a result, the electromagnetic field is not able to leave the interior of the dielectric sphere and keeps circulating returning to the same point with the same phase producing a constructive interference. This mechanism apart from electric resonances, due to the displacement currents, produces magnetic resonances too.

By varying the refractive index, the size and other optical properties of the nanoparticles, it is possible to build nano-structures with the characteristics that suit better the function for which they have been designed. It is possible to choose which wavelength the resonances are produced for, in which regime of the spectrum their optical properties are active...

Another advantage that HRI nanoparticles have with respect to metallic nanoparticles is that they can fulfill the Kerker's scattering conditions: zero forward and zero backward scattering due to coherent effects between the excited electric and magnetic dipolar terms. The possibility of controlling the directionally of the scattered radiation has opened new branches of research concerning nano-antennas, cloaking devices, solar cells, SERS ...

Due to all of these characteristics, high refractive index materials have become one of the most interesting research topic in the field of nanophotonics.

2. OBJECTIVES AND WORK SCHEME

2.1 OBJECTIVES

The main purpose of this work is to analyze the radiative and non radiative contribution to the total scattered field by high refractive index spherical nanoparticles. Through this study it is expected to give an explanation to the red shift and broadening of the resonance peaks of the electric and magnetic scattered field by HRI particles in near field with respect to the far field regime. All this study will be done by means of an approximation in which the HRI particles are considered to behave as an electric dipole crossed to a magnetic dipole.

Another goal of this project is to prove that this approximation is a good approach to consider this problem. In order to achieve this goal, the spectral evolution of the total scattered field by a metallic and a HRI particle calculated by means of the approximation will be compared with the exact solution given by Mie Theory.

For this study an HRI spherical nanoparticle of radius $a=7.5 \text{ mm}$ and $\varepsilon=16$ has been considered. However, a more general analysis has been done too by removing the dependence to the HRI nanoparticle parameters.

Although the dimensions are not in the nanoscale, the results are equivalent to those of a nanoparticle. This re-escalation is due to experimental reasons[8]. The data obtained through these experiments, which are done in the microwave spectral range, have been used as a basis for all the following calculations. Such re-escalation can be done because while $\lambda/(a\varepsilon^{1/2})$ remains constant, the shape of the spectra does not change.

2.2 WORK SCHEME

First of all, a review on the literature concerning the topic of study has been made. This review includes Mie Scattering Theory, the dipole approximation for high refractive index (HRI) spherical nanoparticles, the radiative and non radiative contribution to the electromagnetic fields, the spectral evolution of the localized plasmon resonances in near and far field for metallic nanoparticles, and the Kerker's conditions. Then, the laboratory system in which the calculus were done will be presented so as the computer programs done in order to do all the calculations needed to analyze the topic of this work.

The different steps that will be followed in order to achieve the main objectives of this work are:

- Comparison of the dipole approximation with the exact solution given by Mie theory for a metallic and a HRI nanoparticle.
- Calculation of the intensity of the electric and magnetic field scattered by the electric and magnetic dipole terms of the dipole approximation of a HRI nanoparticle in near and far field.
- Calculation of the intensity of the radiative and non radiative contribution to the electric and magnetic field for a specific and general case of a HRI spherical nanoparticle.
- Calculation of the intensity of the electromagnetic field scattered by the electric and magnetic dipole terms of the dipole approximation of a HRI nanoparticle in near and far field by means of the Poynting vector.
- Calculation of the intensity of the radiative and non radiative components of the scattered electromagnetic waves to the Poynting vector of the electromagnetic field scattered by a HRI nanoparticle.

3. THEORETICAL BACKGROUND

3.1 MIE'S THEORY

Mie's Theory [8] provides a way to calculate the field scattered and absorbed by spheres of arbitrary radius, a , and refractive index, n . By expanding the incident electromagnetic wave into spherical harmonics, Gustav Mie was able to solve the Maxwell equations for this kind of geometry taking into account the boundary condition between the sphere and the medium that surrounds it.

The solutions of the absorbed and scattered fields are developed into vector spherical harmonics. Both solutions depend on different coefficients which are called Mie coefficients. On the one hand there are the scattering coefficients which are usually denoted as a_n and b_n . On the other hand there are the coefficients related to the field inside the sphere, c_n and d_n .

For a linear, homogeneous and isotropic medium, the electromagnetic field must satisfy the Helmholtz equation

$$\nabla^2 \vec{E} + k^2 \vec{E} = 0 \quad \nabla^2 \vec{H} + k^2 \vec{H} = 0 \quad (3.1.1)$$

where \vec{E} and \vec{H} are the electric and magnetic fields and $k = 2\pi n/\lambda$, being n the refractive index of the medium and λ the wavelength of the electromagnetic field.

If the electromagnetic field travels through a free charge medium, the divergence of the electric and the magnetic field is zero

$$\nabla \cdot \vec{E} = 0 \quad \nabla \cdot \vec{H} = 0 \quad (3.1.2)$$

and the relation between the electric and magnetic field is given by

$$\nabla \times \vec{E} = i\omega\mu\vec{H} \quad \nabla \times \vec{H} = i\omega\epsilon\vec{E} \quad (3.1.3)$$

where i is the imaginary unit, ω the angular frequency of the electromagnetic field, μ the magnetic permeability of the medium and ϵ the electric permittivity of the medium.

In order to solve the Helmholtz equation it is convenient to define a new function, \vec{M} , as

$$\vec{M} = \nabla \times (\vec{c} \cdot \psi) \quad (3.1.4)$$

where \vec{c} is a constant vector and ψ an scalar function. The divergence of the function \vec{M} is zero.

Taking into account the relation between the electric and magnetic fields, it is possible to generate another divergence free function from \vec{M} that fulfill the Helmholtz equation

$$\vec{N} = \frac{\nabla \times \vec{M}}{k} \quad (3.1.5)$$

This pair of function, \vec{M} and \vec{N} , are known as the vector harmonics. By means of this functions the initial problem of solving a vectorial differential equation, Helmholtz equation, has been simplified to an easy one, finding the solution to a scalar differential equation

$$\nabla^2 \psi + k^2 \psi = 0 \quad (3.1.6)$$

Because this theory is going to be applied to spheres, the correct set of coordinates to solve this problem are the spherical coordinates. So the scalar function chosen to generate the vector harmonics must satisfy the wave equation in spherical coordinates

$$\frac{1}{r^2} \frac{\partial}{\partial r} \left(r^2 \frac{\partial \psi}{\partial r} \right) + \frac{1}{r^2 \sin \theta} \frac{\partial}{\partial \theta} \left(\sin \theta \frac{\partial \psi}{\partial \theta} \right) + \frac{1}{r^2 \sin^2 \theta} \frac{\partial^2 \psi}{\partial \phi^2} + k^2 \psi = 0 \quad (3.1.7)$$

In order to solve this equation it is necessary to apply the separation of variables method. So the solutions that are being sought, have this form

$$\psi(r, \theta, \phi) = R(r)\Theta(\theta)\Phi(\phi) \quad (3.1.8)$$

which when are substituted into (3.1.7) leads to three separated equations. The solution to these three equations are

$$\begin{aligned} \psi_{omn} &= \cos(m\phi) P_n^m(\cos\theta) z_n(kr) \\ \psi_{emn} &= \sin(m\phi) P_n^m(\cos\theta) z_n(kr) \end{aligned} \quad (3.1.9)$$

where m is an integer, P_n^m are the associated Legendre functions of first kind, of degree n and order m , where $n=m, m+1 \dots$ and z_n represents the spherical Bessel functions. The subscripts o and e indicates either the function has a positive (even) or negative (odd) parity.

By introducing these into the expression (3.1.4 and 3.1.5) the formula of the vector spherical harmonics, $\mathbf{M}^{(l)}_{oin}, \mathbf{M}^{(l)}_{ein}, \mathbf{N}^{(l)}_{oin}, \mathbf{N}^{(l)}_{ein}$, are obtained. This peculiar functions give the normal modes of a spherical particle.

Let a linearly polarized plane wave of wavelength λ be incident on a spherical particle of radius a in the vacuum ($\epsilon=1$). The electric permittivity of the particle is ϵ and its magnetic permeability is μ . In a laboratory coordinate system, the incident electric and magnetic fields are given by

$$\vec{E}_i = E_0 e^{i\vec{k}_i \cdot \vec{r}} \vec{e}_x \quad \vec{H}_i = H_0 e^{i\vec{k}_i \cdot \vec{r}} \vec{e}_y \quad (3.1.10)$$

with a wave propagation direction, $\mathbf{k}=2\pi/\lambda(\sin\alpha \cos\beta, \sin\alpha \sin\beta, \cos\alpha)$.

The expansion of these incident fields into vector spherical harmonics can be expressed as

$$\vec{E}_i = E_0 \sum_{n=1}^{\infty} i^n \frac{2n+1}{n(n+1)} (\vec{M}_{oin}^{(1)} - i\vec{N}_{ein}^{(1)}) \quad \vec{H}_i = -\frac{k}{\omega\mu} E_0 \sum_{n=1}^{\infty} i^n \frac{2n+1}{n(n+1)} (\vec{M}_{ein}^{(1)} - i\vec{N}_{oin}^{(1)}) \quad (3.1.11)$$

where ω is the angular frequency of the field, μ the magnetic permeability of the medium and the super index (1) indicates that the spherical Bessel function of first kind, $j_n(kr)$, should be used for the calculus of the vector spherical harmonics $\mathbf{M}^{(l)}_{oin}, \mathbf{M}^{(l)}_{ein}, \mathbf{N}^{(l)}_{oin}, \mathbf{N}^{(l)}_{ein}$.

Therefore, the scattered field is

$$\vec{E}_S = E_0 \sum_{n=1}^{\infty} i^n \frac{2n+1}{n(n+1)} (ia_n \vec{N}_{ein}^{(3)} - b_n \vec{M}_{oin}^{(3)}) \quad \vec{H}_S = \frac{1}{\mu_0 c} \sum_{n=1}^{\infty} i^n \frac{2n+1}{n(n+1)} (ib_n \vec{N}_{oin}^{(3)} + a_n \vec{M}_{ein}^{(3)}) \quad (3.1.12)$$

where the super index (3) indicates that the spherical Hankel function, $h_n^{(l)}$, may be used for the calculus of the vector spherical harmonics of these expansions.

The scattering coefficients, a_n and b_n , can be expressed as a function of the Ricatti-Bessel functions

$$\psi_n(\rho) = \rho j_n(\rho) \quad \xi_n(\rho) = \rho h_n^{(1)}(\rho) \quad (3.1.13)$$

For a non magnetic medium the expressions of the scattering coefficients are

$$a_n = \frac{m\psi_n(mx)\psi_n'(x) - \psi_n(x)\psi_n'(mx)}{m\psi_n(mx)\xi_n'(x) - \xi_n(x)\psi_n'(mx)} \quad b_n = \frac{\psi_n(mx)\psi_n'(x) - m\psi_n(x)\psi_n'(mx)}{\psi_n(mx)\xi_n'(x) - m\xi_n(x)\psi_n'(mx)} \quad (3.1.14)$$

where x is the size parameter and m is the relative refractive index defined by

$$x = \frac{2\pi a}{\lambda} \quad m = \frac{n_{sphere}}{n_{medium}} \quad (3.1.15)$$

In addition, the expansion in terms of the Mie scattering coefficients gives us a multipolar expansion of the field. The a_n coefficients represent the electrical contribution whereas the b_n coefficients represent the magnetic contribution to the scattered field. The subindex n indicates which multipole we are considering. For example, $n=1$ represents the dipole term, $n=2$ the quadrupole terms, $n=3$ the octupole terms and so on.

By evaluating them as function of the wavelength it is easy to know which wavelength the resonances are produced for. For example, the wavelength that makes a_1 maximum is the one at which the electric dipole resonance is produced.

A related magnitude with the scattering problem is the scattering efficiency, Q_{sca} . This scattering efficiency gives the relation between the interaction and the particle cross sections. It can also be defined the extinction efficiency, Q_{ext} . Both magnitudes can be expressed in terms of the Mie scattering coefficients as

$$Q_{ext} = \frac{2}{x^2} \sum_{n=1}^{\infty} (2n+1) \text{Re}(a_n + b_n) \quad Q_{sca} = \frac{2}{x^2} \sum_{n=1}^{\infty} (2n+1) (|a_n|^2 + |b_n|^2) \quad (3.1.16)$$

Due to energy conservation, the extinguished radiation may be equal to the sum of the scattered and absorbed radiation. As a result of this, it is possible to give an expression for the absorption efficiency, Q_{abs} .

$$Q_{abs} = Q_{ext} - Q_{sca} \quad (3.1.17)$$

3.2 DIPOLE APPROXIMATION FOR METALLIC AND HIGH REFRACTIVE INDEX NANOPARTICLES

Metallic and high refractive index (HRI) nanoparticles with size much smaller than the wavelength show different behavior when they are illuminated. While metallic ones only present electric dipole resonances, HRI nanoparticles can show both electric and magnetic dipole resonances. In terms of the Mie Theory, the behavior of metallic particles is dominated by the scattering coefficient a_1 . Usually, for this kind of particles the b_1 coefficient is negligible. However, for HRI particles, a_1 and b_1 are necessary to explain their scattering behavior.

Although the exact solution of the scattered field by spheres of arbitrary size and refractive index is given by Mie Theory, it is possible to use an approximation for metallic and HRI nanoparticles to calculate their scattered field when their size is much smaller than the wavelength of the incident light.

By using this approximation, particles are modeled as dipoles. In the case of the metallic nanoparticles, because they only present electric dipole resonances, they are considered as electric dipoles. On the contrary, HRI nanoparticles are considered as an electric dipole perpendicular to a magnetic dipole because they show electric and magnetic dipole resonances.

Because the electric and magnetic fields radiated by electric and magnetic dipoles are well known, it is easy to obtain the total scattered field by metallic and HRI nanoparticles. In addition, by using this approximation it is easier to separate the electric from the magnetic response of the nanoparticles.

The expressions for the electric and magnetic fields radiated by an electric dipole, $\vec{E}_{S\ elec}$ and $\vec{H}_{S\ elec}$, are respectively given by [9]

$$\vec{E}_{S\ elec}(\vec{r}) = \frac{1}{4\pi\epsilon_0} \left[\vec{p} \left(k^2 - \frac{1}{r^2} + \frac{ik}{r} \right) + \vec{n}(\vec{n} \cdot \vec{p}) \left(-k^2 + \frac{3}{r^2} + \frac{3ik}{r} \right) \right] \frac{e^{ikr}}{r} \quad (3.2.1)$$

$$\vec{H}_{S\ elec}(\vec{r}) = \frac{1}{4\pi\sqrt{\mu_0\epsilon_0}} \left[(\vec{n} \times \vec{p}) \frac{e^{ikr}}{r} \left(k^2 + \frac{ik}{r} \right) \right] \quad (3.2.2)$$

The expressions for the electric and magnetic fields radiated by a magnetic dipole, $\vec{E}_{S\ mag}$ and $\vec{H}_{S\ mag}$, are respectively given by [9]

$$\vec{E}_{S\ mag}(\vec{r}) = -\frac{1}{4\pi} \sqrt{\frac{\mu_0}{\epsilon_0}} (\vec{n} \times \vec{m}) \frac{e^{ikr}}{r} \left(k^2 + \frac{ik}{r} \right) \quad (3.2.3)$$

$$\vec{H}_{S\ mag}(\vec{r}) = \frac{1}{4\pi} \left[\vec{m} \left(k^2 - \frac{1}{r^2} + \frac{ik}{r} \right) + \vec{n}(\vec{n} \cdot \vec{m}) \left(-k^2 + \frac{3}{r^2} - \frac{3ik}{r} \right) \right] \frac{e^{ikr}}{r} \quad (3.2.4)$$

where \vec{p} and \vec{m} are

$$\vec{p} = \epsilon_0 \alpha_E E_0 \quad \alpha_E = \frac{i6\pi a_1}{k^3} \quad (3.2.5.a) \quad (3.2.6.a)$$

$$\vec{m} = \alpha_M H_0 \quad \alpha_M = \frac{i6\pi b_1}{k^3} \quad (3.2.5.b) \quad (3.2.6.b)$$

and a_l and b_l are the Mie scattering coefficients.

For metallic nanoparticles, because they are modeled as electric dipoles, the total electric and magnetic scattered fields are given by

$$\vec{E}_S(\vec{r}) = \vec{E}_{S\text{ elec}}(\vec{r}) \quad (3.2.7)$$

$$\vec{H}_S(\vec{r}) = \vec{H}_{S\text{ elec}}(\vec{r}) \quad (3.2.8)$$

However, due to the fact that HRI nanoparticles are modeled as an electric dipole perpendicular to a magnetic dipole, the total electric and magnetic scattered fields are

$$\vec{E}_S(\vec{r}) = \vec{E}_{S\text{ elec}}(\vec{r}) + \vec{E}_{S\text{ mag}}(\vec{r}) \quad (3.2.9)$$

$$\vec{H}_S(\vec{r}) = \vec{H}_{S\text{ elec}}(\vec{r}) + \vec{H}_{S\text{ mag}}(\vec{r}) \quad (3.2.10)$$

This formulation of the electric and magnetic scattered fields provides an easy way to separate the electric and magnetic dipolar contributions to them. By taking the electric and magnetic fields scattered by the magnetic dipole equal to zero, $\vec{E}_{S\text{ mag}}(\mathbf{r})=0$ and $\vec{H}_{S\text{ mag}}(\mathbf{r})=0$, only the electric dipolar term is being considered. On the contrary, by taking the electric and magnetic fields scattered by the electric dipole equal to zero, $\vec{E}_{S\text{ elec}}(\mathbf{r})=0$ and $\vec{H}_{S\text{ elec}}(\mathbf{r})=0$, only the magnetic dipolar term is being considered in this approximation.

In the next figure shows how the electric and magnetic dipoles are oriented depending on the linear polarization of the incoming electromagnetic field. The electric dipole (blue arrow) is considered to be parallel to the linear polarization of the electric field. The same thing happens with the magnetic dipole in the case of HRI nanoparticles, for which the magnetic dipole is considered to be in the same direction as the linear polarization of the magnetic field. The displacement current generated by the magnetic dipole is represented by the blue circle.

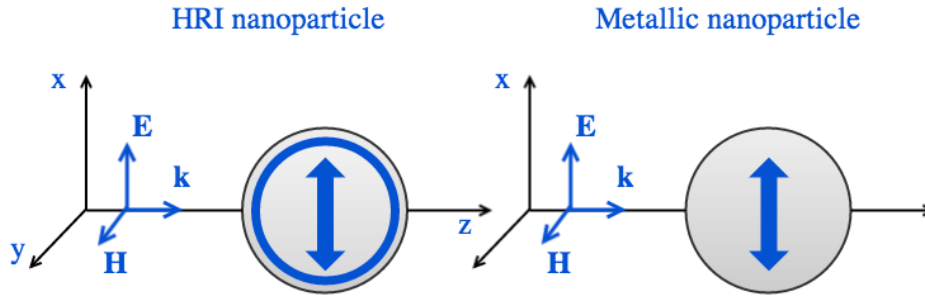


Figure 3.1. Representation of the dipole approximation for a high refractive index (HRI) and a metallic nanoparticle. It is shown the orientation of the electric dipole (blue arrow) and the displacement current produced by the magnetic dipole (blue circle) for a determined linear polarization of the incoming electromagnetic field.

3.3 RADIATIVE AND NON RADIATIVE CONTRIBUTION

The *angular spectrum representation* [10] is a method used to solve propagation, radiation, scattering and diffraction problems by expanding the electromagnetic field into plane waves. The scattered field by spheres can be expanded into its radiative and non radiative contribution by using this representation. Whereas the radiative contribution takes the main role in far field optics, the non radiative contribution cannot be neglected in near field optics.

Let's consider a monochromatic scalar wavefield propagating in a source free region of the space with $z > 0$. The spatial part of the wavefield, $U(r)$, satisfies the Helmholtz equation

$$\nabla^2 U + k^2 U = 0 \quad \text{for } z \geq 1 \quad (3.3.1)$$

We assume that at any z -constant plane the wavefield, $U(r)$, has a Fourier transform given by the next formula

$$U(x, y, z) = \int \int_{-\infty}^{\infty} \tilde{U}(p, q, m) e^{ik(px+qy)} dpdq \quad (3.3.2)$$

By introducing this expression into the Helmholtz equation one obtains

$$\frac{\partial^2}{\partial z^2} \tilde{U}(p, q, z) + k^2 m^2 \tilde{U}(p, q, z) = 0 \quad (3.3.3)$$

where

$$m = \sqrt{1 - p^2 - q^2} \quad \text{for } p^2 + q^2 \leq 1 \quad (3.3.4.a)$$

$$m = i\sqrt{p^2 + q^2 - 1} \quad \text{for } p^2 + q^2 > 1 \quad (3.3.4.b)$$

There are two solutions for the differential equation (3.3.3)

$$\tilde{U}_1(p, q, z) = a(p, q) e^{ikmz} \quad \tilde{U}_2(p, q, z) = b(p, q) e^{-ikmz} \quad (3.3.5)$$

By introducing these expressions into the equation (3.3.2), we obtain

$$U(x, y, z) = \int \int_{-\infty}^{\infty} a(p, q) e^{ik(px+qy+mz)} dpdq \quad V(x, y, z) = \int \int_{-\infty}^{\infty} b(p, q) e^{ik(px+qy-mz)} dpdq \quad (3.3.6)$$

These expressions are the angular spectrum representations of the wavefield in the source free half space. The first one corresponds to plane waves components propagating into $z \geq 0$ whereas in the second one the plane waves components are propagating into $z \leq 0$.

When m takes real values, (3.3.4.a), the components are called *homogenous or radiative*. On the contrary, if m takes imaginary values, (3.3.4.b) the components are called *inhomogenous or non radiative*. These inhomogenous components are also called *evanescent waves* and their amplitude decay exponentially along the z -axis.

The angular spectrum of the wavefield propagating through $z > 0$ in spherical coordinates takes a very useful form that allows us to solve problems that involve spheres. In this case, the polar angles characterize the components of the unit vector $s=(p,q,m)$.

$$p=(\sin\alpha \cos\beta) \quad (3.3.7.a)$$

$$q=(\sin\alpha \sin\beta) \quad (3.3.7.b)$$

$$m=\cos\alpha. \quad (3.3.7.c)$$

The β angle is real and takes values between $[-\pi, \pi]$. However α may take imaginary values. The α angle depends on the value of m (equation (3.3.7.c)). On the one hand, as p^2+q^2 grows from $p^2+q^2=0$ to $p^2+q^2=1$ (equation (3.3.4.a)) α takes values between $[0, \pi/2]$. On the other hand, when p^2+q^2 takes values that fulfill the condition $p^2+q^2>1$, m takes imaginary values (equation (3.3.4.b)) in the interval $[0, i\infty]$. However, if $\alpha = \pi/2 - i\delta$ then $m = \cos(\pi/2 - i\delta) = i \sinh\delta$ which also grows from $m=0$ to $m=i\infty$. So for $p^2+q^2>1$, α takes values as $\alpha = \pi/2 - i\delta$.

As a result, the angular spectrum of the wavefield propagating through $z > 0$ in spherical coordinates is given by

$$U(\vec{r}) = \frac{ik}{2\pi} \int_{-\pi}^{\pi} d\beta \int_0^{\frac{\pi}{2} - i\delta} d\alpha \sin\alpha F(\alpha, \beta) e^{ik\vec{s}\cdot\vec{r}} \quad (3.3.8)$$

The second integral can be divided into two parts: the one with a real integrating angle, which corresponds to the radiative contribution, and the one with an imaginary integrating angle, which corresponds to the non radiative contribution.

This expression can be particularized for the case of the electromagnetic field scattered by a sphere in terms of a multipolar expansion [11]. The angular spectrum of plane waves of the scattered field by a sphere is given by

$$\vec{E}_s(\vec{r}) = \frac{1}{2\pi} \int_{-\pi}^{\pi} d\beta \int_0^{\frac{\pi}{2} - i\infty} d\alpha \sin\alpha [S_1(\cos\alpha)\cos\beta\vec{e}_\alpha - S_2(\cos\alpha)\sin\beta\vec{e}_\beta] e^{ik\vec{r}} \quad (3.3.9.a)$$

$$\vec{H}_s(\vec{r}) = \frac{1}{2\pi} \int_0^{2\pi} d\beta \int_0^{\frac{\pi}{2} - i\infty} d\alpha \sin\alpha [S_2(\cos\alpha)\sin\beta\vec{e}_\alpha + S_1(\cos\alpha)\cos\beta\vec{e}_\beta] e^{ik\vec{r}} \quad (3.3.9.b)$$

where the angular spectra $S_1(\cos\alpha)$ and $S_2(\cos\alpha)$ are

$$S_1(\cos\alpha) = \sum_{n=1}^{\infty} \frac{2n+1}{n(n+1)} [a_n \pi_n(\cos\alpha) + b_n \tau_n(\cos\alpha)] \quad S_2(\cos\alpha) = \sum_{n=1}^{\infty} \frac{2n+1}{n(n+1)} [a_n \tau_n(\cos\alpha) + b_n \pi_n(\cos\alpha)] \quad (3.3.10)$$

where π_n and τ_n are the angle-depend function from Mie scattering.

Because we are interested in magnetodielectric particles, only the terms with $n=1$ will be considered. This terms only take into account the electric and magnetic dipolar contributions.

Finally, the angular spectrum of plane waves of the scattered field by a magnetodielectric particle can be written in terms of a_1 and b_1 as

$$\vec{E}_s(\vec{r}) = \frac{3a_1}{4\pi} \int_0^{2\pi} d\beta \int_0^{\frac{\pi}{2} - i\infty} d\alpha \sin\alpha (\cos\beta\vec{e}_\alpha - \cos\alpha \sin\beta\vec{e}_\beta) e^{ik\vec{r}} + \frac{3b_1}{4\pi} \int_0^{2\pi} d\beta \int_0^{\frac{\pi}{2} - i\infty} d\alpha \sin\alpha (\cos\alpha \cos\beta\vec{e}_\alpha - \sin\beta\vec{e}_\beta) e^{ik\vec{r}}$$

$$\vec{H}_s(\vec{r}) = \frac{3a_1}{4\pi} \int_0^{2\pi} d\beta \int_0^{\frac{\pi}{2} - i\infty} d\alpha \sin\alpha (\cos\alpha \sin\beta\vec{e}_\alpha + \cos\beta\vec{e}_\beta) e^{ik\vec{r}} + \frac{3b_1}{4\pi} \int_0^{2\pi} d\beta \int_0^{\frac{\pi}{2} - i\infty} d\alpha \sin\alpha (\sin\beta\vec{e}_\alpha + \cos\alpha \cos\beta\vec{e}_\beta) e^{ik\vec{r}} \quad (3.3.11)$$

This equations are expressed in such a way that the response of the electric and the magnetic dipole can be easily separated. By considering $a_l=0$, only the electromagnetic field scattered by the magnetic dipole is being considered. On the contrary, if $b_l=0$, only the electromagnetic field scattered by the electric dipole is being considered. For example, when the radiative and non radiative contribution to the scattered field by a metallic nanoparticles under the dipole approximation is being calculated, $b_l=0$ is considered in the equations (3.3.11).

In the laboratory coordinate system (see figure 3.2) $\mathbf{k}=\frac{2\pi}{\lambda}(\sin\alpha \cos\beta, \sin\alpha \sin\beta, \cos\alpha)$, $\mathbf{e}_\alpha=(\cos\alpha \cos\beta, \cos\alpha \sin\beta, -\sin\alpha)$ and $\mathbf{e}_\beta=(-\sin\beta, \cos\beta, 0)$. By dividing the coordinate α into two intervals, $[0, \pi/2]$ and $[\pi/2-i0, \pi/2+i0]$, the radiative and non radiative contribution can be obtained.

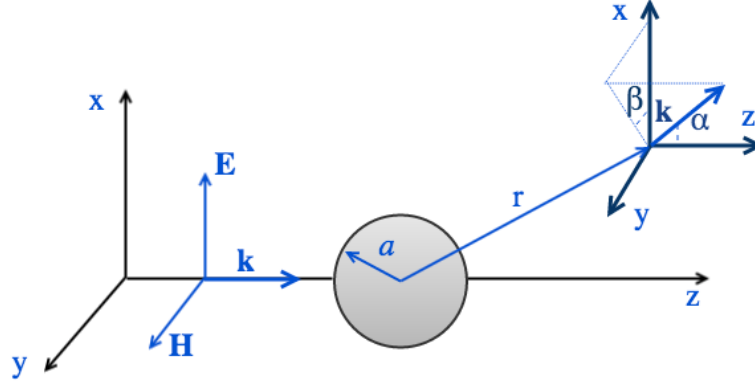


Figure 3.2. Scheme of the laboratory system considered during the calculus. A HRI spherical particle has been placed in the origin of a laboratory coordinate system. It has been illuminated with a plane wave electromagnetic field traveling in the z-direction. At a point r the contribution of the plane wave with wave vector $k(\alpha, \beta)$ to the angular spectrum of the scattered field is also represented.

Then, the total scattered field can be expressed in terms of the radiative and non radiative contribution as

$$\vec{E}_S = \vec{E}_S^R + \vec{E}_S^{N-R} \quad \vec{H}_S = \vec{H}_S^R + \vec{H}_S^{N-R} \quad (3.3.12)$$

where \vec{E}_S^R represents the radiative contribution and \vec{E}_S^{N-R} represents the non radiative contribution.

However, due to the arduousness of the evaluation of the non radiative integral, this contribution is obtain by the subtraction of the total scattered field and the radiative contribution.

$$\vec{E}_S^{N-R} = \vec{E}_S - \vec{E}_S^R \quad \vec{H}_S^{N-R} = \vec{H}_S - \vec{H}_S^R \quad (3.3.13)$$

In the following calculations the square modulus of the electric, $|\vec{E}|^2$, and the magnetic fields, $|\vec{H}|^2$, are going to be analyzed. By calculating this magnitude from equation 3.3.12, it is obtained

$$|\vec{E}_S|^2 = |\vec{E}_S^R|^2 + |\vec{E}_S^{N-R}|^2 + 2\text{Re}(\vec{E}_S^{N-R} * \vec{E}_S^R) \quad (3.3.14)$$

$$|\vec{H}_S|^2 = |\vec{H}_S^R|^2 + |\vec{H}_S^{N-R}|^2 + 2\text{Re}(\vec{H}_S^{N-R} * \vec{H}_S^R) \quad (3.3.15)$$

As it can be seen, the intensity of the total scattered field is not just the sum of the intensities of both contributions. A interference term between the radiative and non radiative contribution has to be added too.

3.4 SPECTRAL BEHAVIOR OF LOCALIZED PLASMON RESONANCES IN NEAR AND FAR FIELD FOR METALLIC NANOPARTICLES.

When the spectral evolution of the LSP peaks produced in metallic nanoparticles are studied in the near and far field regimes, two main differences are observed: The LSP near field peak is red shifted with respect to the LSP far field peak. In addition, a broadening of the peak is produced in the transition from far to near field [6]. This features can be seen in the next figures, where the scattered field by a silver nanoparticle of radius $a=25\text{ nm}$ has been calculated at the point $(a,0,0)$ in the near and far field (see *Figure 4.1*) regimens.

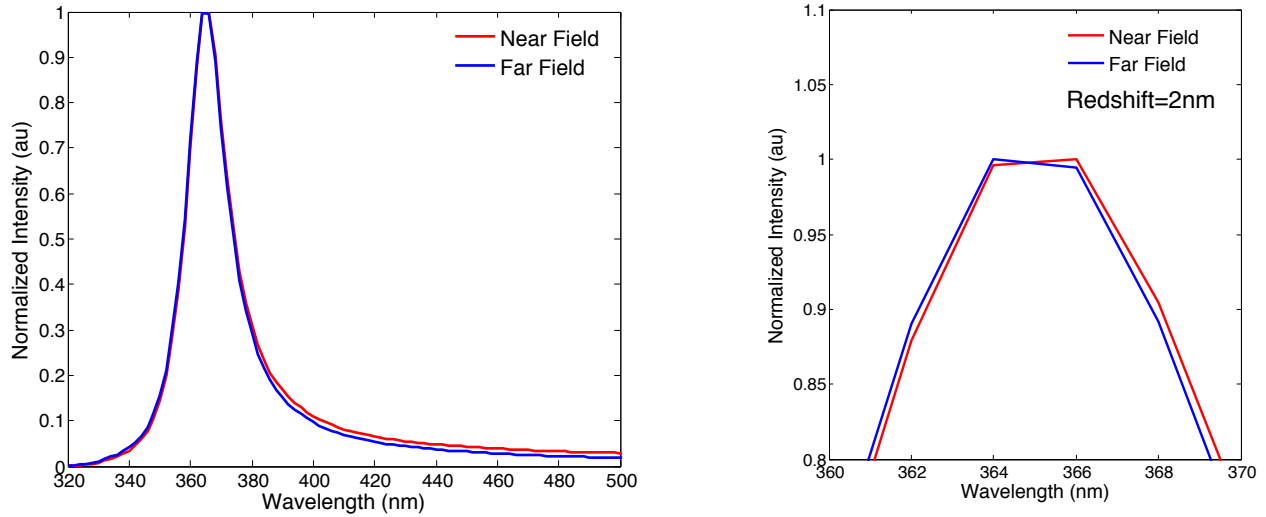


Figure 3.3. Spectral evolution of the total scattered field by a silver nanoparticle of radius $a=25\text{ nm}$ calculated at the point $(a,0,0)$, in the near and far field regime. A broadening and a red shift of the near field LSP peak with respect to the far field LSP peak can be seen.

This phenomenon can be explained in terms of the radiative and non radiative contribution to the total scattered field [6]. The non radiative contribution composed mainly of evanescent waves keeps attached to the surface of the scatterer. As the distance from the scatterer increases, the amplitude of these waves decreases exponentially and the radiative part of the scattered wave starts to dominate.

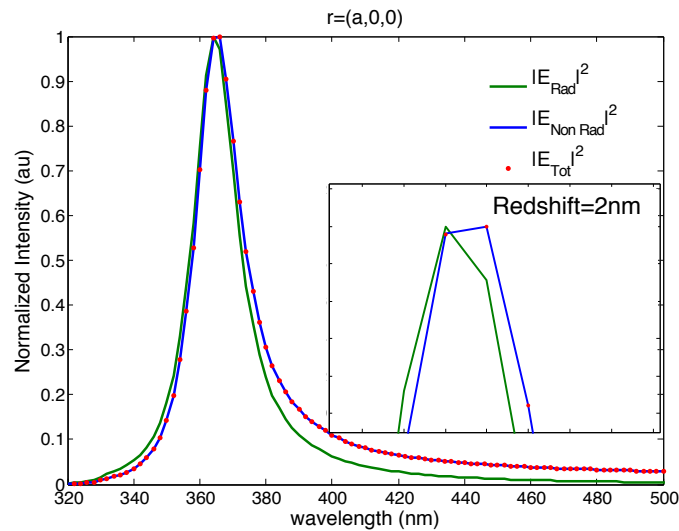


Figure 3.4. Spectral evolution of $|E_{Rad}|^2$ (green solid line), $|E_{Non Rad}|^2$ (blue solid line) and $|E_{Tot}|^2$ (red dots) at the point $(a,0,0)$ of a spherical silver nanoparticle with $a=25\text{nm}$.

As it can be seen in *Figure 3.4*, the spectral evolution of the total scattered field matches exactly the one of the non radiative contribution. In addition, it can be seen how the total and non radiative contribution resonance peak is redshifted and broader than the peak of the radiative contribution.

Figure 3.5 shows a more general study of this phenomenon. In this plot the dependence with the particle parameters has been suppressed by dividing the different contributions by the Mie scattering coefficient a_1 . This parameter is the one who contains all the particle information (size and refractive index). So this plot shows the universal behavior of metallic nanoparticles.

One of the features that are clearly represented in *Figure 3.5* is that in near field the non radiative contribution takes the lead roll while the radiative contribution is negligible. In addition, it is important to point out that the interference between the radiative and non radiative contribution is also negligible.

Due to the fact that in near field the non radiative contribution resonance peak is red shifted and broader than the resonance peak of radiative contribution, and it dominates over the latter, the evanescent waves could be responsible of the broadening and the redshift observed in *Figure 3.3*.

Figure 3.5 also shows an universal dependence on the incident wavelength under the dipole approximation. This universal law determines that while the incident wavelength increases, so does $|E_{Non\ Rad}/a_1|^2$ following a power law λ^n with $n \approx 6$. In the far field regime the radiative contribution follows a power law with $n \approx 2$ as the Rayleigh approximation dictates [8].

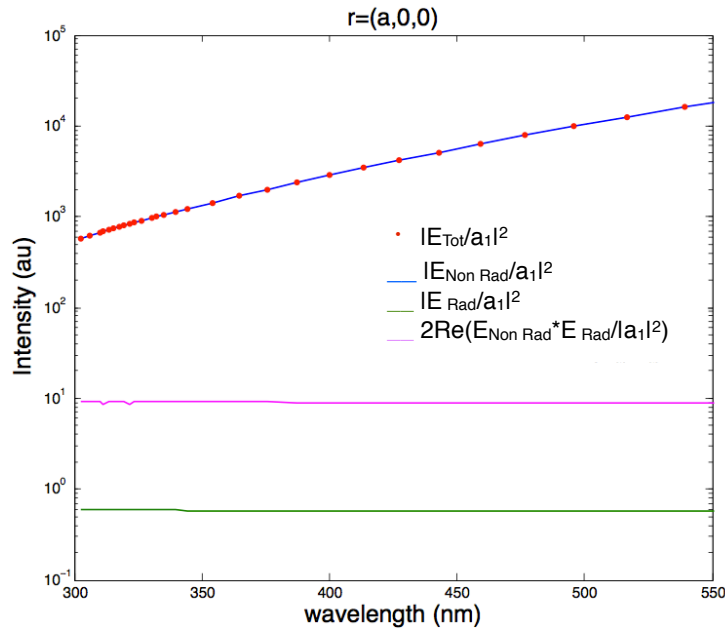


Figure 3.5. Spectral evolution of $|E_{Rad}/a_1|^2$ (green solid line), $|E_{Non\ Rad}/a_1|^2$ (blue crosses) and $|E_{Tot}/a_1|^2$ (red dots) at the point $(a,0,0)$ where a is the radius of the nanoparticle. The interference between contributions is also represented by a magenta line. The blue line represents the numerical fitting of the spectral evolution of the non radiative contribution to a power law $a+b\lambda^{5.8}$.

Another factor that takes an important role in this phenomenon is the magnitude of the imaginary part of the electric permittivity, ϵ_i , in the spectral range in which the study is done. Materials like gallium or nickel with a high ϵ_i suffer a bigger red shift than those with low ϵ_i as silver, gold or aluminum.

3.5 KERKER'S CONDITIONS

In the early eighties Kerker et al. [13] showed that the light scattered by spherical particles with magnetic properties ($\mu \neq 1$) presents unusual scattering properties. A particle with this characteristics shows both electric and magnetic resonances that can be expressed in terms of the Mie scattering coefficients a_n and b_n .

When $a_1 = b_1$, the electric permittivity is equal to the magnetic permeability, ($\mu = \varepsilon$), and the zero backward scattering condition is fulfilled. Under this condition the intensity of the backscattered light is zero (see *Figure 3.6 (left)*). However, when $a_1 = -b_1$, the electric permittivity has opposite sign to the magnetic permeability, ($\mu = -\varepsilon$), and the zero forward scattering condition is achieved (see *Figure 3.6 (right)*).

If we consider high refractive index nanoparticles, the scattered field can be described as an electric and magnetic dipole with Mie scattering terms a_1 and b_1 . As a result it is also possible to observe the Kerker's conditions [12] in this type of particles.

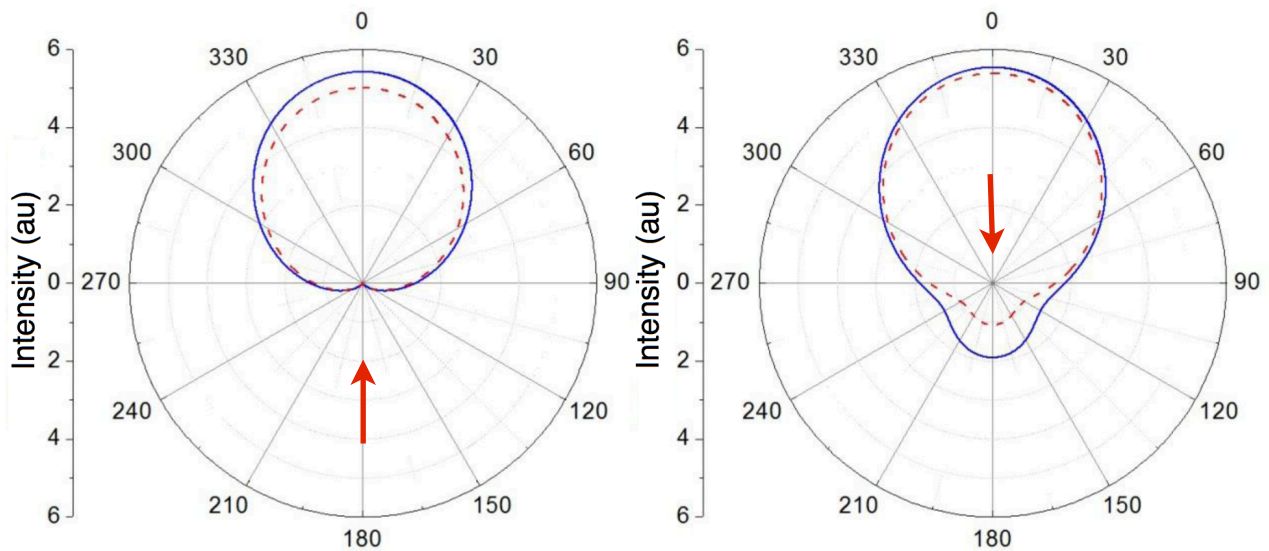


Figure 3.6. Polar representation of the intensity of the scattered electromagnetic field by a high refractive particle when it is fulfilled the zero backward condition (left) or the zero forward condition (right). The red arrow represents the direction in which the particle is being illuminated.

4. RESULTS

In this section the results of the calculus will be exposed as well as their physical interpretation. In addition, a brief explanation of the laboratory system considered during the calculus and the programs created to do them will be given.

4.1 LABORATORY SYSTEM

In all the analyzed situations a spherical HRI particle of radius $a= 7.5mm$ with constant refractive index $n=4$ has been considered. The particle has been illuminated by a plane wave electromagnetic field. This incident electromagnetic field has been considered to travel in the z -direction, with the electric field linearly polarized along the x -direction and the magnetic field linearly polarized along the y -direction (see *Figure 3.2*).

In *Figure 3.2* is also represented the contribution in a r distant point of a plane wave to the angular spectrum of the scattered field. The calculus made of the radiative and non radiative contributions are made by taking into account this reference frame and coordinates α and β .

For the dipole approximation in the case of the metallic particles, the electric dipole will be considered to be oriented along the x -direction. In the case of HRI nanoparticles, the electric dipole will be considered to be oriented along the x -direction and the magnetic dipole along the y -direction (see *Figure 3.1*).

All the calculation will be done in two different points of the particle: $(a,0,0)$ and $(0,0,a)$. These two points have been chosen because for the electric dipole resonances the hot spot is produced at $(a,0,0)$ and the minimum at $(0,0,a)$ (see *Figure 4.1*).

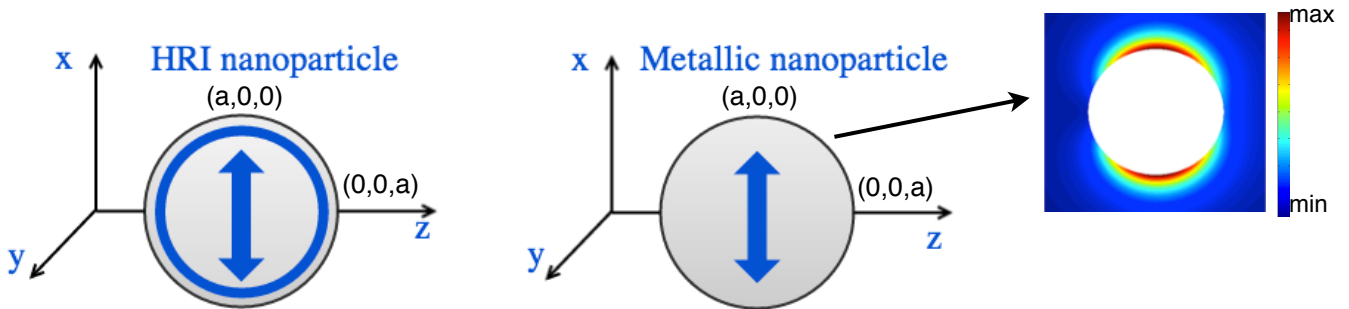


Figure 4.1. Scheme of the orientation of the dipoles taken during the calculus for HRI and metallic nanoparticles using the dipole approximation. With a blue arrow is represented the electric dipole whereas with the blue circle is represented the displacement current produced by the magnetic dipole. The points $(a,0,0)$ (hotspot) and $(0,0,a)$ (minimum) are the places where all the calculations are going to be done. The color map represents the intensity of the scattered electric field near the surface of the scatterer (near field distribution).

4.2 COMPUTER PROGRAMS

In order to calculate the radiative and non radiative contribution to the total electric scattered field a computer program using Matlab programming language has been done. It is formed by different functions:

- ***coeficiente_an_no_vacio.m***: calculate the Mie scattering coefficient a_n from incoming parameters as the wavelength, radius and refractive index of the particle, refractive index of the medium and order n .
- ***coeficiente_bn_no_vacio.m***: calculate the Mie scattering coefficient b_n from incoming parameters as the wavelength, radius and refractive index of the particle, refractive index of the medium and order n .
- ***campo_dipolos_cualquier_punto.m***: calculate the intensity of the electric field scattered by an electric and a magnetic dipole both crossed at any point of space in the laboratory system. The incoming parameters are the wavelength, refractive index and radius of the particle, refractive index of the medium and the point of space in which the calculus is done.
- ***campo_homo_cualquier_punto.m***: calculate the intensity of the homogenous contribution of the electric field at any point of space. The incoming parameters are the wavelength, refractive index and radius of the particle, refractive index of the medium and the point of space in which the calculus is done.
- ***campo_inhomo_cualquier_punto.m***: calculate the intensity of the inhomogenous contribution of the electric field in any point of space. The incoming parameters are the wavelength, refractive index and radius of the particle, refractive index of the medium and the point of space in which the calculus is done.
- ***inter_cualquier_punto.m***: calculate the interference of the homogenous and inhomogenous contributions in any point of space. The incoming parameters are the wavelength, refractive index and radius of the particle, refractive index of the medium and the point of space in which the calculus is done.
- ***pinta_homo_inhomo_dip.m***: plot in the same figure all the contributions. The incoming parameters are the wavelength, refractive index and radius of the particle, refractive index of the medium and the point of space in which the calculus is done.
- ***plot_field***: calculate and plot the intensity of the electric field scattered by a spherical particle in the XZ plane considering the Dipole Approximation. The incoming parameters are the wavelength, refractive index and radius of the particle, and a matrix with the evaluation points in the XZ plane.
- ***plot_field_homo***: calculate and plot the intensity of the radiative contribution to the electric field scattered by a spherical particle in the XZ plane considering the Dipole Approximation. The incoming parameters are the wavelength, refractive index and radius of the particle, and a matrix with the evaluation points in the XZ plane.
- ***plot_field_inhomo***: calculate and plot the intensity of the non radiative contribution to the electric field scattered by a spherical particle in the XZ plane considering the Dipole Approximation. The incoming parameters are the wavelength, refractive index and radius of the particle, and a matrix with the evaluation points in the XZ plane.
- ***plot_field_inter***: calculate and plot the interference of the homogenous and inhomogenous contributions in the XZ plane. The incoming parameters are the wavelength, refractive index and radius of the particle, and a matrix with the evaluation points in the XZ plane.

Similar programs have been done in order to calculate the radiative and non radiative contribution to the total magnetic scattered field.

The HRI nanoparticles have been modeled as two dipoles. In order to know the behavior of the electric and magnetic fields scattered by the isolated electric dipole, some computer programs have been created in order to achieve this goal. The whole program has been programmed with Matlab programming language and it is made from several functions which are presented below:

- ***campo_elec_dipolo_elec_isolated.m***: calculate the electric field scattered by a spherical nanoparticle modeled as a electric dipole at any point of space. It also calculate its intensity and intensity normalized to the Mie coefficient a_1 . The incoming parameters are the wavelength, refractive index and radius of the particle, refractive index of the medium and the point of space in which the calculus is done.
- ***campo_elec_inhomogeneo_dip_elec_isolated.m***: calculate the non radiative contribution to the electric field scattered by a spherical nanoparticle modeled as a electric dipole at any point of space. It also calculate its intensity and intensity normalized to the Mie coefficient a_1 . The incoming parameters are the wavelength, refractive index and radius of the particle, refractive index of the medium and the point of space in which the calculus is done.
- ***campo_elec_homogeneo_dip_elec_isolated.m***: calculate the radiative contribution to the electric field scattered by a spherical nanoparticle modeled as a electric dipole at any point of space. It also calculate its intensity and intensity normalized to the Mie coefficient a_1 . The incoming parameters are the wavelength, refractive index and radius of the particle, refractive index of the medium and the point of space in which the calculus is done.
- ***campo_elec_inter_dip_elec_isolated.m***: calculate the interference between the radiative and non radiative contribution of the total electric scattered field by a spherical nanoparticle modeled as a electric dipole at any point of space . The incoming parameters are the wavelength, refractive index and radius of the particle, refractive index of the medium and the point of space in which the calculus is done.
- ***campo_mag_dipolo_elec_isolated.m***: calculate the magnetic field scattered by a spherical nanoparticle modeled as a electric dipole at any point of space. It also calculate its intensity and intensity normalized to the Mie coefficient a_1 . The incoming parameters are the wavelength, refractive index and radius of the particle, refractive index of the medium and the point of space in which the calculus is done.
- ***campo_mag_inhomogeneo_dip_elec_isolated.m***: calculate the non radiative contribution to the magnetic field scattered by a spherical nanoparticle modeled as a electric dipole at any point of space. It also calculate its intensity and intensity normalized to the Mie coefficient a_1 . The incoming parameters are the wavelength, refractive index and radius of the particle, refractive index of the medium and the point of space in which the calculus is done.
- ***campo_mag_homogeneo_dip_elec_isolated.m***: calculate the radiative contribution to the magnetic field scattered by a spherical nanoparticle modeled as a electric dipole at any point of space. It also calculate its intensity and intensity normalized to the Mie coefficient a_1 . The incoming parameters are the wavelength, refractive index and radius of the particle, refractive index of the medium and the point of space in which the calculus is done.
- ***campo_mag_inter_dip_elec_isolated.m***: calculate the interference between the radiative and non radiative contribution of the total magnetic scattered field by a spherical nanoparticle modeled as a electric dipole at any point of space . The incoming parameters are the wavelength, refractive index and radius of the particle, refractive index of the medium and the point of space in which the calculus is done.
- ***poyniting_total_dip_elec_isolated.m***: calculate the Poynting vector of the total field scattered by a spherical nanoparticle modeled as a electric dipole at any point of space. The incoming parameters are the wavelength, refractive index and radius of the particle, refractive index of the medium and the point of space in which the calculus is done.

- ***poyniting_vec_homo_dip_elec_isolated.m***: calculate the Poynting vector of the radiative contribution to the total field scattered by a spherical nanoparticle modeled as a electric dipole at any point of space. The incoming parameters are the wavelength, refractive index and radius of the particle, refractive index of the medium and the point of space in which the calculus is done.
- ***poyniting_vec_inhomo_elec_isolated.m***: calculate the Poynting vector of the non radiative contribution to the total field scattered by a spherical nanoparticle modeled as a electric dipole at any point of space. The incoming parameters are the wavelength, refractive index and radius of the particle, refractive index of the medium and the point of space in which the calculus is done.
- ***pinta_cualquier_punto_elec_dip_elec_isolated_div_an.m***: plot the intensity of the electric field, its radiative and non radiative contribution normalized to a_1 scattered by a spherical nanoparticle modeled as a electric dipole at any point of space. The incoming parameters are the wavelength, refractive index and radius of the particle, refractive index of the medium and the point of space in which the calculus is done.
- ***pinta_cualquier_punto_elec_dip_elec_isolated.m***: plot the intensity of the electric field, its radiative and non radiative contribution scattered by a spherical nanoparticle modeled as a electric dipole at any point of space. The incoming parameters are the wavelength, refractive index and radius of the particle, refractive index of the medium and the point of space in which the calculus is done.
- ***pinta_cualquier_punto_mag_dip_elec_isolated_div_an.m***: plot the intensity of the magnetic field, its radiative and non radiative contribution normalized to a_1 scattered by a spherical nanoparticle modeled as a electric dipole at any point of space. The incoming parameters are the wavelength, refractive index and radius of the particle, refractive index of the medium and the point of space in which the calculus is done.
- ***pinta_cualquier_punto_mag_dip_elec_isolated.m***: plot the intensity of the magnetic field, its radiative and non radiative contribution scattered by a spherical nanoparticle modeled as a electric dipole at any point of space. The incoming parameters are the wavelength, refractive index and radius of the particle, refractive index of the medium and the point of space in which the calculus is done.

Similar programs have been done to study the electric and magnetic fields scattered by the isolated magnetic dipole. In this case the normalization have been done to b_1 .

For doing the comparison between the exact method, Mie Theory, and the dipole approximation, another computer program has been done. This program like the previous ones have been programmed using Matlab. The different functions that make the whole program are:

- ***plot_field.m***: calculate and plot the intensity of the electric field scattered by a spherical particle in the XZ plane considering the Dipole Approximation. The incoming parameters are the wavelength, refractive index and radius of the particle, and a matrix with the evaluation points in the XZ plane.
- ***plot_field_mag.m***: calculate and plot the intensity of the magnetic field scattered by a spherical particle in the XZ plane considering the Dipole Approximation. The incoming parameters are the wavelength, refractive index and radius of the particle, and a matrix with the evaluation points in the XZ plane.
- ***MIE_field.m***: calculate and plot the intensity of the electric field scattered by a spherical particle at any point considering Mie Theory. The incoming parameters are the wavelength, refractive index and radius of the particle, and a matrix with the evaluation plane.
- ***MIE_field_mag.m***: calculate and plot the intensity of the magnetic field scattered by a spherical particle at any point considering Mie Theory. The incoming parameters are the wavelength, refractive index and radius of the particle, and a matrix with the evaluation points.

- *MIE_spectral_evolution_elec.m*: calculate the spectral evolution of the scattered electric field. The incoming parameters are the wavelength, refractive index and radius of the particle, refractive index of the medium and the point of space in which the calculus is done.
- *MIE_spectral_evolution_mag.m*: calculate the spectral evolution of the scattered magnetic field. The incoming parameters are the wavelength, refractive index and radius of the particle, refractive index of the medium and the points of space in which the calculus is done.

4.3 COMPARISON BETWEEN MIE THEORY AND THE DIPOLE APPROXIMATION

The exact solution for the scattered field by spherical particles of arbitrary size and refractive index is given by the Mie theory. However, it is possible to treat metallic and high refractive index dielectric nanoparticles using the dipole approximation as it was commented in section (3.2). In order to know if this approximation is a good approach to the problem which is going to be analyzed, both methods are going to be compared.

The spectral evolution of the total electric and magnetic fields scattered by metallic and HRI nanoparticles will be calculated using Mie theory and the dipole approximation. The spectral evolution is a representation of the intensity of the scattered field versus the wavelength of the incident electromagnetic field. This representation is very common in the field of nanoplasmonics because it allows us to see in an easy way for which wavelength the resonances are produced.

4.3.1 METALLIC NANOPARTICLES

For the calculus of the spectral evolution of metallic nanoparticles it has been considered a silver nanoparticle with a radius of $a=25\text{ nm}$. The point of space at which the calculations have been done are $(a,0,0)$ and $(0,0,a)$ (see Figure 4.1), where the electric field reaches its maximum (hot spot) and minimum intensity respectively. The wavelength range used goes from 300 to 500 nm.

As it is seen in the next plots, only the electric dipole resonance is present in all the spectral evolutions that have been calculated. This is the expected behavior since metallic nanoparticles have been considered to behave as electric dipoles when their size is smaller than the incident wavelength.

Another interesting thing is that the calculations using the dipole approximation match perfectly the exact solution given by Mie theory. As a result, the dipole approximation is a good approach to the study of metallic nanoparticles with size much smaller than the incident wavelength.

Finally, as it was predicted by the expression of the magnetic field scattered by the electric dipole (equation (3.2.2)), the intensity of the magnetic field is zero at $(a,0,0)$ (see Figure 4.3 (left)).

- Spectral evolution of the scattered electric field:

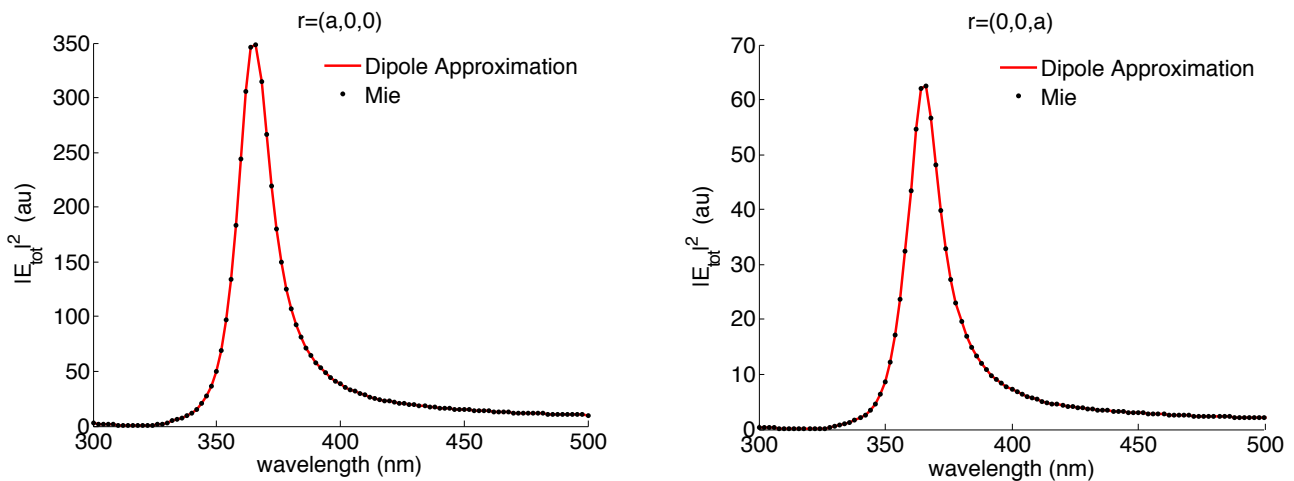


Figure 4.2. Spectral evolution of the electric field scattered by a metallic nanoparticle made of silver which has a radius of $a=25\text{nm}$. The calculus has been done at $(a,0,0)$ and $(0,0,a)$ by means of Mie theory (black dots) and the dipole approximation (red line).

- Spectral evolution of the scattered magnetic field:

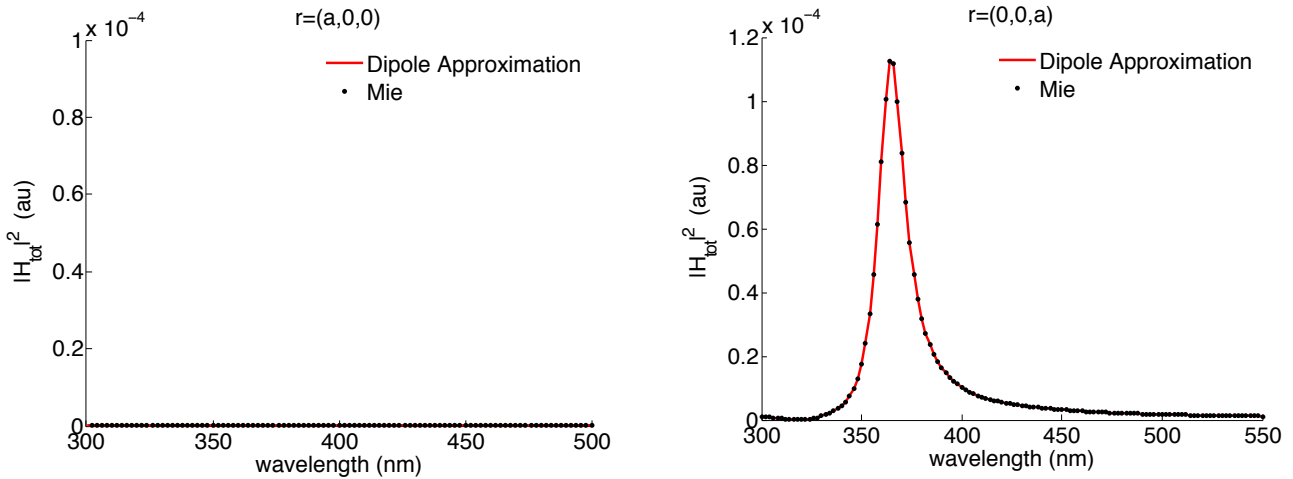


Figure 4.3. Spectral evolution of the magnetic field scattered by a metallic nanoparticle made of silver which has a radius of $a=25\text{nm}$. The calculus has been done at $(a,0,0)$ and $(0,0,a)$ by means of Mie theory (black dots) and the dipole approximation (red line).

Another thing that can be observed is how the intensity of the electric field is several orders of magnitude bigger than the intensity of the magnetic field.

4.3.2 HIGH REFRACTIVE INDEX NANOPARTICLES

For the calculus of the spectral evolution of high refractive index nanoparticles it has been considered a nanoparticle with a radius of $a=7,5\text{mm}$ and an electric permittivity $\epsilon=16$. The point of space in which the calculations have been done are $(a,0,0)$ and $(0,0,a)$. The wavelength range used goes from the 40 to the 70 mm.

As it is shown in the next plots, both the electric and magnetic dipole resonances can be seen. The electric dipole resonance is produced at around 46mm , whereas the magnetic dipole resonance is produced at around 62mm . This is the expected behavior since we have considered the HRI nanoparticles as an electric dipole crossed to a magnetic dipole.

Once again, the results that have been obtained by means of the dipole approximation match perfectly with the exact solution given by Mie theory. So the dipole approximation is a good approach to the study of high refractive index nanoparticles too.

- Spectral evolution of the scattered electric field:

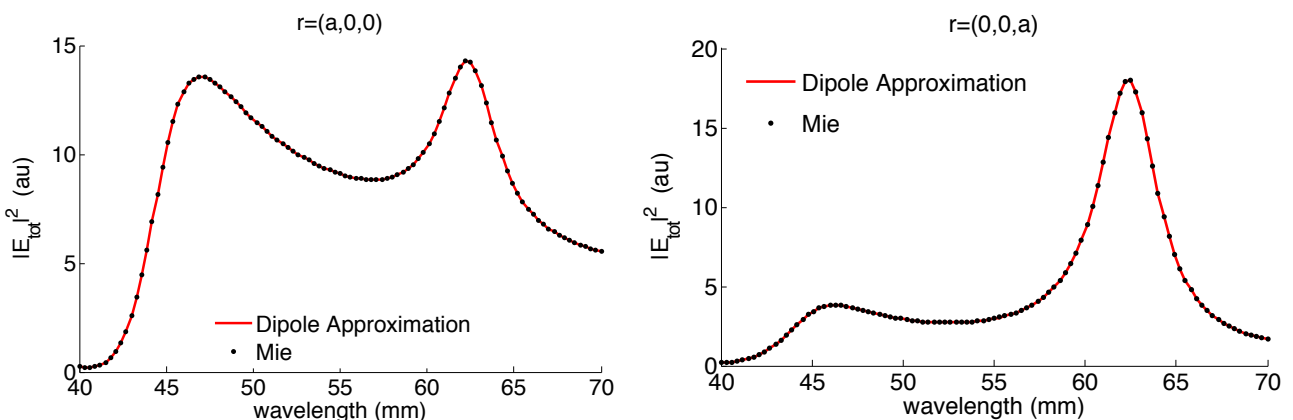


Figure 4.4. Spectral evolution of the electric field scattered by a high refractive index nanoparticle which has a radius of $a=7,5\text{mm}$ and $\epsilon=16$. The calculus has been done at $(a,0,0)$ and $(0,0,a)$ by means of Mie theory (black dots) and the dipole approximation (red line).

- Spectral evolution of the scattered magnetic field:

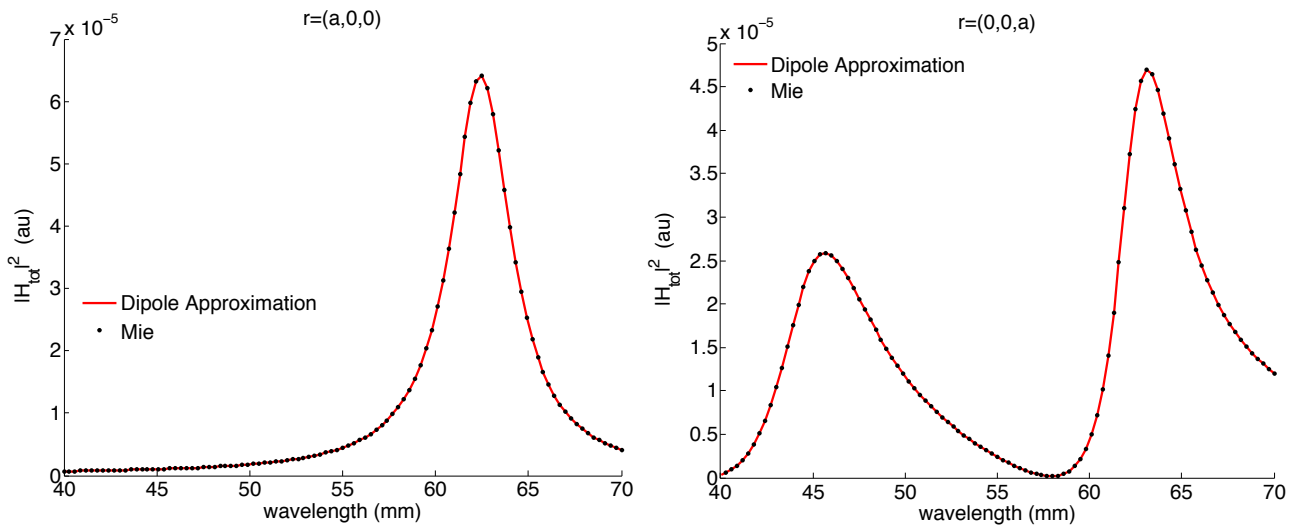


Figure 4.5. Spectral evolution of the magnetic field scattered by a high refractive index nanoparticle which has a radius of $a=7,5\text{mm}$ and $\epsilon=16$. The calculus has been done at $(a,0,0)$ and $(0,0,a)$ by means of Mie theory (black dots) and the dipole approximation (red line).

Once again, it can be seen how the intensity of the electric field is several orders of magnitude bigger than the intensity of the magnetic field.

4.4 SPECTRAL BEHAVIOR OF THE DIPOLE RESONANCES OF HRI NANOPARTICLES IN NEAR AND FAR FIELD.

High refractive index nanoparticles not only do they show electric dipole resonances, but also magnetic dipole ones. These scatterers can be modeled as an electric dipole crossed to a magnetic one, following the dipole approximation explained in section (3.2). As in the case of the metallic nanoparticles, section (3.4), the resonances peaks are different in the near and far field regimes.

4.4.1 SPECTRAL EVOLUTION OF THE ELECTRIC SCATTERED FIELD IN NEAR AND FAR FIELD.

The next plots show the intensity of the total scattered electric field by the electric and magnetic dipoles as a function of the wavelength of the incident field at the electric and magnetic dipole resonances in near (red line) and far field (blue line) regimens.

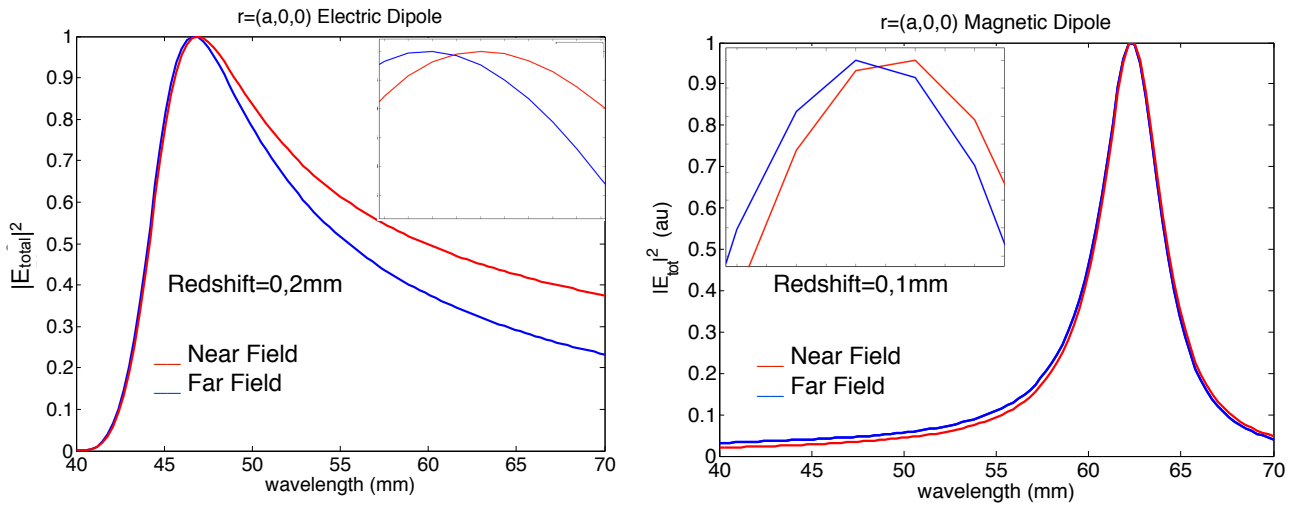


Figure 4.6. Spectral evolution of the total electric scattered field by the electric (left) and magnetic dipoles (right) in the near (red solid line) and far field regimes (blue solid line) at the point $(a,0,0)$. For the calculus an HRI nanoparticle with $a=7.5$ mm and $\epsilon=16$ has been considered.

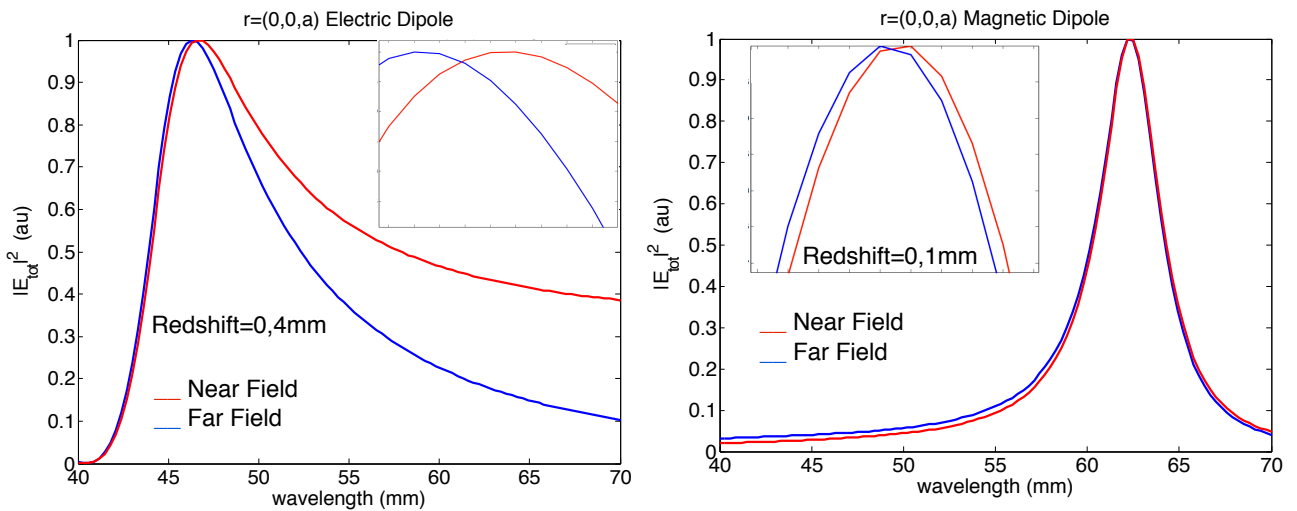


Figure 4.7. Spectral evolution of the total electric scattered field by the electric (left) and magnetic dipoles (right) in the near (red solid line) and far field regimes (blue solid line) at the point $(0,0,a)$. For the calculus an HRI nanoparticle with $a=7.5$ mm and $\epsilon=16$ has been considered.

The electric and magnetic dipole shows very different behaviors. The peaks for the electric dipole resonance in near field are broader and redshifted with respect to those in the far field regime. However, the peaks for the magnetic dipole resonance in near field are not broader, and less red shifted than in the far field regime.

4.4.2 SPECTRAL EVOLUTION OF THE MAGNETIC SCATTERED FIELD IN NEAR AND FAR FIELD.

In the next plots are shown the intensity of the total magnetic scattered field by the electric and magnetic dipoles as function of the wavelength at the electric and magnetic dipole resonances in near (red line) and far field (blue line).

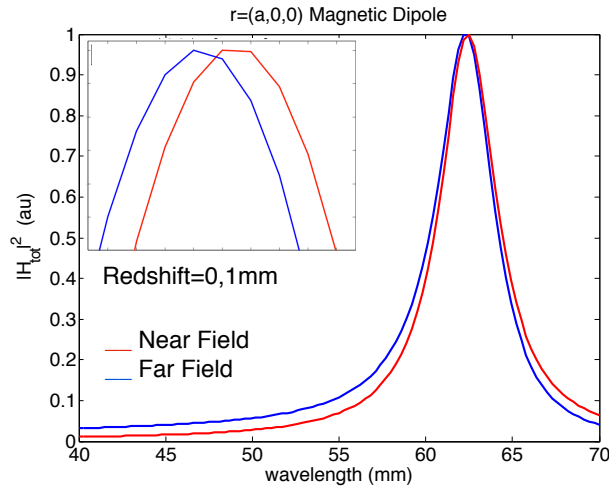


Figure 4.8 Spectral evolution of the total magnetic scattered field by the magnetic dipoles in the near (red solid line) and far field regimes (blue solid line) at the point $(a,0,0)$. For the calculus an HRI nanoparticle with $a=7.5$ mm and $\epsilon=16$ has been considered.

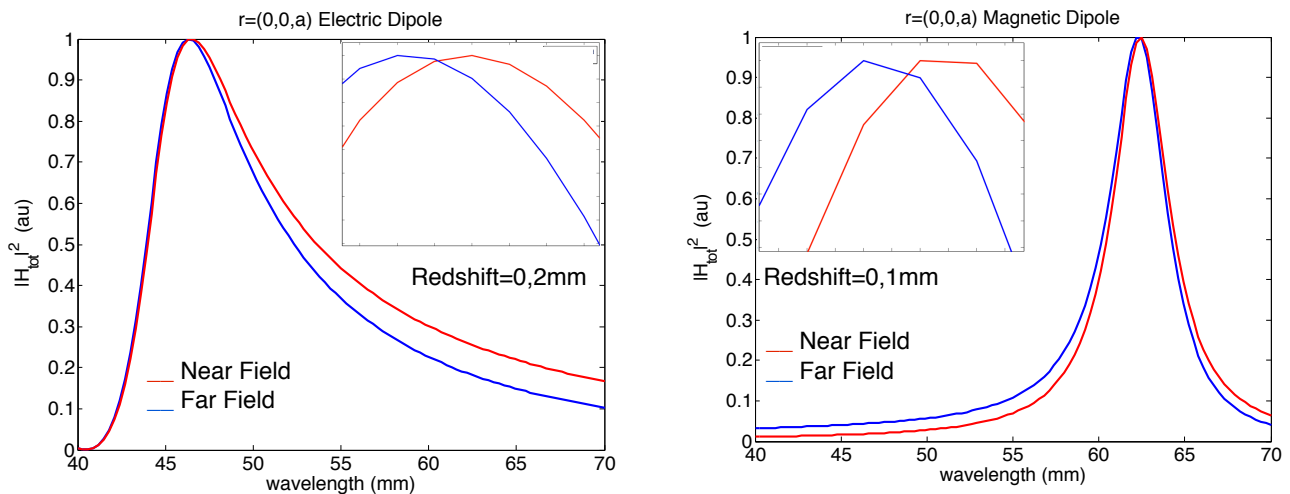


Figure 4.9. Spectral evolution of the total electric scattered field by the electric (left) and magnetic dipoles (right) in the near (red solid line) and far field regimes (blue solid line) at the point $(0,0,a)$. For the calculus an HRI nanoparticle with $a=7.5$ mm and $\epsilon=16$ has been considered.

In this case, the peaks at the electric dipole resonance in near field are broader and red shifted with respect to the ones in the far field regimes. However, the peaks at the magnetic dipole resonance in near field are redshifted with respect to the far field regime but they are not broader.

4.4.3 RADIATIVE AND NON RADIATIVE CONTRIBUTION TO THE ELECTRIC FIELD SCATTERED BY HIGH REFRACTIVE INDEX NANOPARTICLES IN NEAR FIELD.

In this section we will discuss the radiative and non radiative contribution to the total scattered electric field in the near field regime. As it has been outlined before, in far field the total field is dominated by the radiative contribution. However, as it will be seen now, in near field the non radiative contribution takes the lead role.

In the next figures, an specific case of a HRI index particle of $\epsilon=16$ is studied. The spectral evolution of the total scattered electric field (red line), its radiative (green line) and non radiative contribution (blue line) and the interference (pink line) between both contributions has been calculated at two different points, $(a,0,0)$ and $(0,0,a)$ (see Figure 4.1), for a range of wavelengths between 40 and 70 mm.

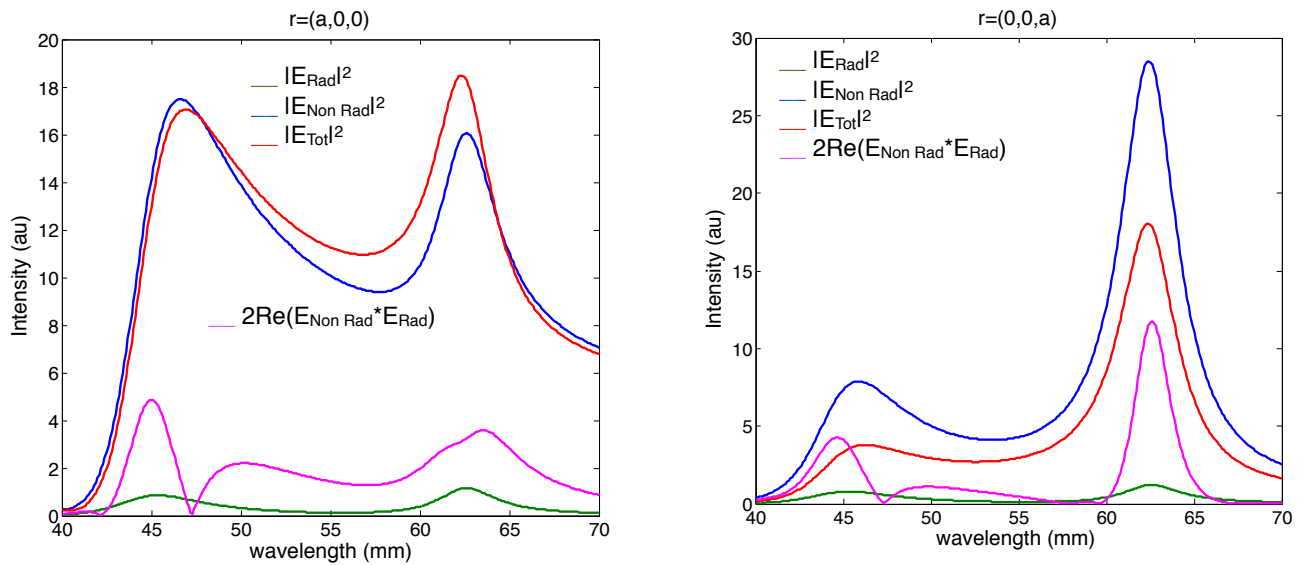


Figure 4.10. Spectral evolution of the radiative (green line), non radiative (blue line) contribution as well as their interference (magenta line) to the electric scattered field. The total electric scattered field is represented by the red solid line. All the contributions have been calculated in the points $r=(a,0,0)$ (left), and $r=(0,0,a)$ (right).

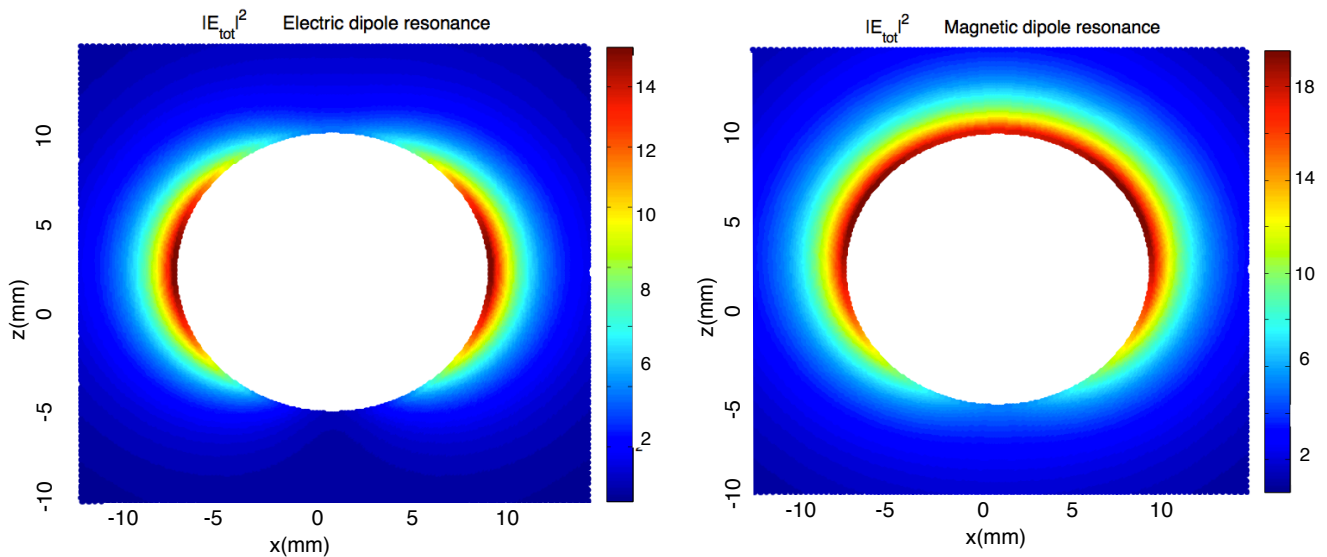


Figure 4.11. Intensity of the electric field scattered by an HRI spherical particle of radius $a=7.5\text{mm}$ and refractive index $n=4$. The excitation wavelength is $\lambda \approx 46.5\text{ mm}$ (left) and $\lambda=62\text{ mm}$ (right). This wavelength corresponds with the electric dipole excitation wavelength (left) and the magnetic dipole excitation wavelength (right).

Figure 4.10 shows two important features. The first one related to the resonance peaks and the other one to the intensity of the different contributions.

First, as it was expected since an HRI particle is being considered, there are two resonance peaks. The electric dipole resonance is produced at $\lambda \approx 46.5 \text{ mm}$ and the magnetic dipole resonance produced at $\lambda \approx 62 \text{ mm}$. The electric dipole resonance peak at $(a,0,0)$ is much intense than at $(0,0,a)$. However, the magnetic dipole resonance peaks have similar intensities at both positions. This can be explained taking into account the geometrical configuration (Figure 4.1 left) considered for each dipole in the dipole approximation (see section 4.1). The electric dipole is considered along the x -direction, so in the direction $(1,0,0)$ the intensity of the total scattered electric field is maximum. On the contrary, in the perpendicular direction, $(0,0,1)$, it takes its minimum value (see Figure 4.11 left). The magnetic dipole, chosen along the y -direction, due to its circular symmetry scatters the electric field with the same intensity at both points (see Figure 4.11 right).

Another important thing that Figure 4.10 shows is that the non radiative contribution dominates over the radiative contribution. However, the latter is not negligible as in the case of metallic nanoparticles. The interference between both contributions for HRI is also not negligible unlike for metallic nanoparticles.

By decomposing the scattered field into the electric and the magnetic dipolar terms in the dipole approximation, it is possible to see how the total and the non radiative contributions are red shifted with respect to the radiative contribution (Figure 4.12 and Figure 4.13). Due to the fact that the radiative contribution dominates over the non radiative contribution in the far field regime, the evanescent waves can be responsible for this red shift.

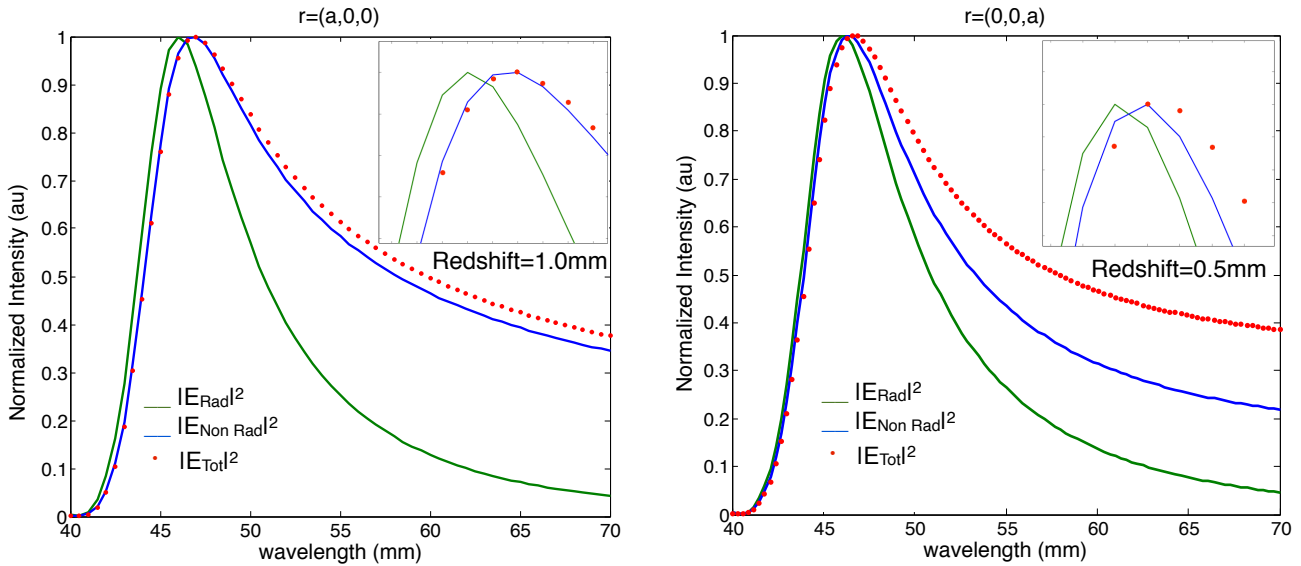


Figure 4.12. Normalized spectral evolution of the electric scattered field (red dots) and its radiative (green solid line) and non radiative contribution (blue solid line). The electric field is considered to be scattered by the electric dipolar term of the dipole approximation for an HRI with radius $a=7.5 \text{ mm}$ and $\epsilon=16$. The calculus has been done in two different points: $(a,0,0)$ (left) and $(0,0,a)$ (right).

In far field, where the radiative contribution dominates, the peaks are narrower than in near field (see Figure 4.6 (left) and Figure 4.7 (left)). Due to the fact that in near field the non radiative contribution is also broader than the radiative contribution, and it dominates over the latter, the evanescent waves could be also responsible of the broadening.

The red shift of the radiative contribution with respect to the non radiative contribution and total electric scattered field by the magnetic dipolar term (figure 4.13), is much smaller than in the case of the electric dipolar term (figure 4.12). In addition, no broadening of the peaks can be appreciated.

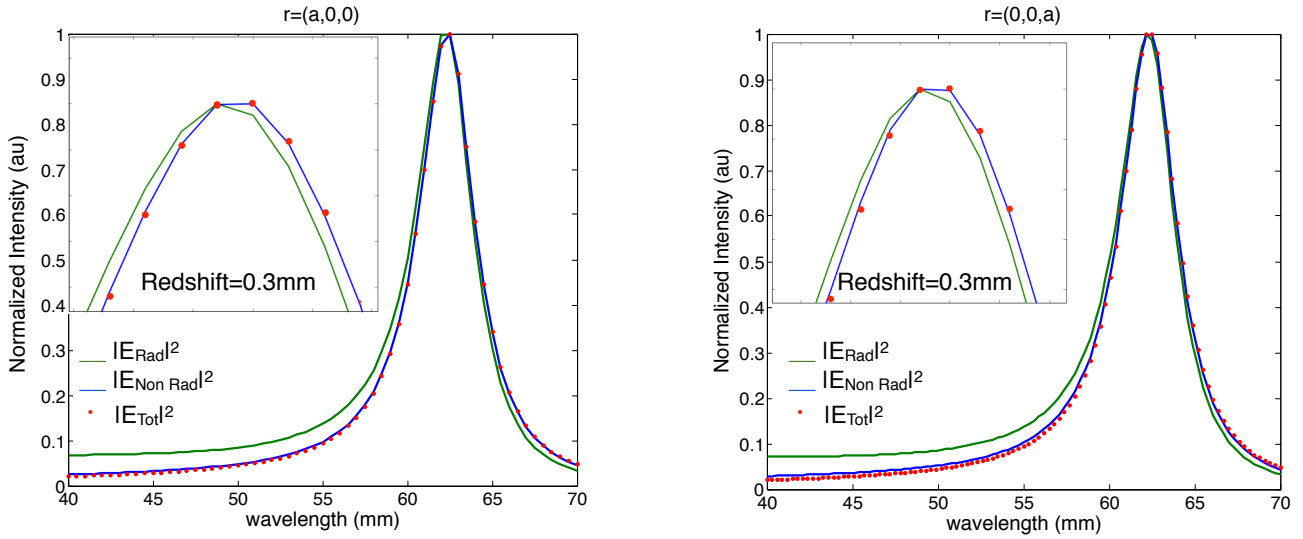


Figure 4.13. Normalized spectral evolution of the electric scattered field (red dots) and its radiative (green solid line) and non radiative contribution (blue solid line). The electric field is considered to be scattered by the magnetic dipolar term of the dipole approximation for an HRI with radius $a=7.5$ mm and $\epsilon=16$. The calculus has been done in two different points: $(a,0,0)$ (left) and $(0,0,a)$ (right).

Although for the electric dipolar term the non radiative contribution does not exactly matches the total scattered field, in the case of the magnetic dipolar term they are nearly equal (see Figure 4.13). The discrepancy between the non radiative and the total scattered fields can be produced by the interference between the radiative and non radiative contribution. This term that was negligible for metals it is not for HRI particles.

Until now the analysis of this phenomena has been done considering an HRI spherical nanoparticle of radius $a=7.5$ mm and $\epsilon=16$. In order to do a more general analysis, the dependence with the nanoparticle parameters will be removed by normalizing to the Mie scattering coefficients in the equation 3.3.11: a_l in the case of the electric dipolar term and b_l for the magnetic dipolar term of the dipole approximation.

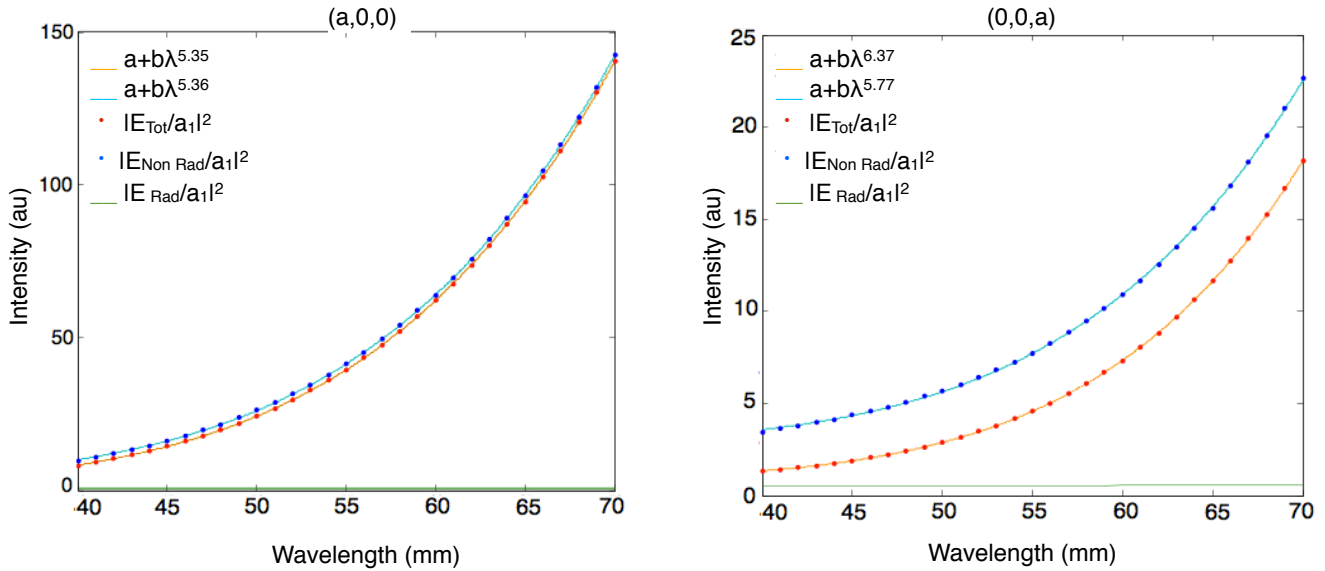


Figure 4.14. Spectral evolution of $|E_{tot}/a_1|^2$ (red dots), $|E_{non rad}/a_1|^2$ (blue dots) and $|E_{rad}/a_1|^2$ (green line) at two positions, $(a,0,0)$ (left) and $(0,0,a)$ (right). The orange and the fair blue solid line represents the numeral fitting of the spectral evolution of the total and non radiative contribution to a function $a+b\lambda^n$. In the case of the point $(a,0,0)$ for the total scattered field $n=5.37$ and for the non radiative contribution $n=5.36$. In the case of the point $(0,0,a)$ for the total scattered field $n=6,37$ and for the non radiative contribution $n=5.77$.

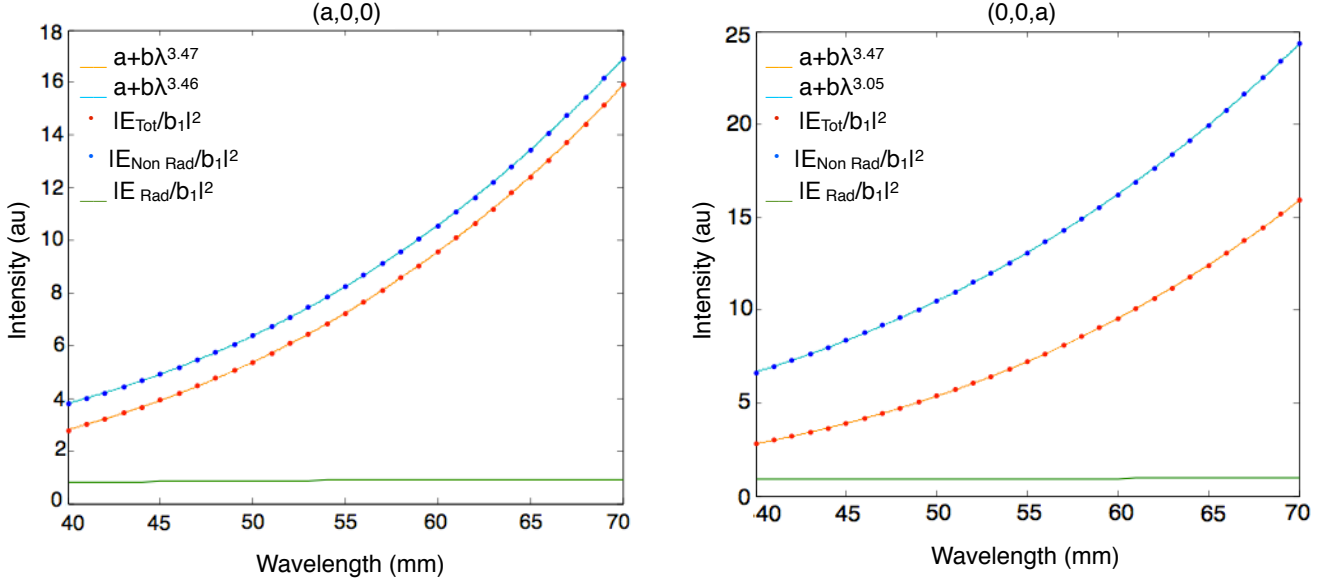


Figure 4.15. Spectral evolution of $|E_{tot}/b_1|^2$ (red dots), $|E_{non\ rad}/b_1|^2$ (blue dots) and $|E_{rad}/b_1|^2$ (green line) at two positions, $(a,0,0)$ (left) and $(0,0,a)$ (right). The orange and the fair blue solid line represents the numeral fitting of the spectral evolution of the total and non radiative contribution to a function $a+b\lambda^n$. In the case of the point $(a,0,0)$ for the total scattered field $n=3.47$ and for the non radiative contribution $n=3.46$. In the case of the point $(0,0,a)$ for the total scattered field $n=3.47$ and for the non radiative contribution $n=3.05$.

Figure 4.14 and figure 4.15 show two important features. First, in near field, the non radiative contribution dominates over the radiative one. This can be seen by comparing the blue dots with the green solid line. However, the total scattered field does not match the non radiative contribution. This difference is caused by the interference between the radiative and non radiative contributions.

In addition, by the numerical fitting, it can be seen how the total scattered field and its non radiative contribution show an universal dependence with the wavelength. In the case of the electric field scattered by the electric dipolar term of the dipole approximation (Figure 4.14) at the point $(a, 0,0)$, both the total and non radiative contribution follow a power law $a+b\lambda^n$ with $n\approx 5$. At the point $(0,0,a)$ the exponent is $n\approx 6$. This behavior in near field differs from far field where the total field scales at $a+b\lambda^n$ with $n\approx 2$.

Also, for the electric field scattered by the magnetic dipolar term of the dipole approximation (Figure 4.15), an universal dependence with the wavelength can be observed. However, in this case it does not matter the point we considered; the total electric field scales at $a+b\lambda^n$ with $n\approx 3.5$. This was the expected result since the magnetic dipole scatters equally in the $(a, 0,0)$ and $(0,0,a)$ points as it can be seen in Figure 4.11 (right). Once again the near field behavior differs from the far field behavior, where the power law followed by the scattered field is $a+b\lambda^n$ with $n\approx 2$. In the case of the non radiative contribution, it also follows a universal dependence with the wavelength as a power law. At the point $(a,0,0)$ $n\approx 3.5$ and at $(0,0,a)$ $n\approx 3$.

4.4.4 RADIATIVE AND NON RADIATIVE CONTRIBUTION TO THE MAGNETIC FIELD SCATTERED BY HIGH REFRACTIVE INDEX NANOPARTICLES IN NEAR FIELD.

In this section we will discuss the radiative and non radiative contribution to the total magnetic scattered field in the near field regime for a HRI particle.

In the next figures, an specific case of a HRI index particle of $\varepsilon=16$ is studied. The spectral evolution of the total scattered magnetic field, its radiative and non radiative contribution, and the interference between them has been calculated at two different points, $(a,0,0)$ and $(0,0,a)$, and for a range of wavelengths between 40 and 70 mm.

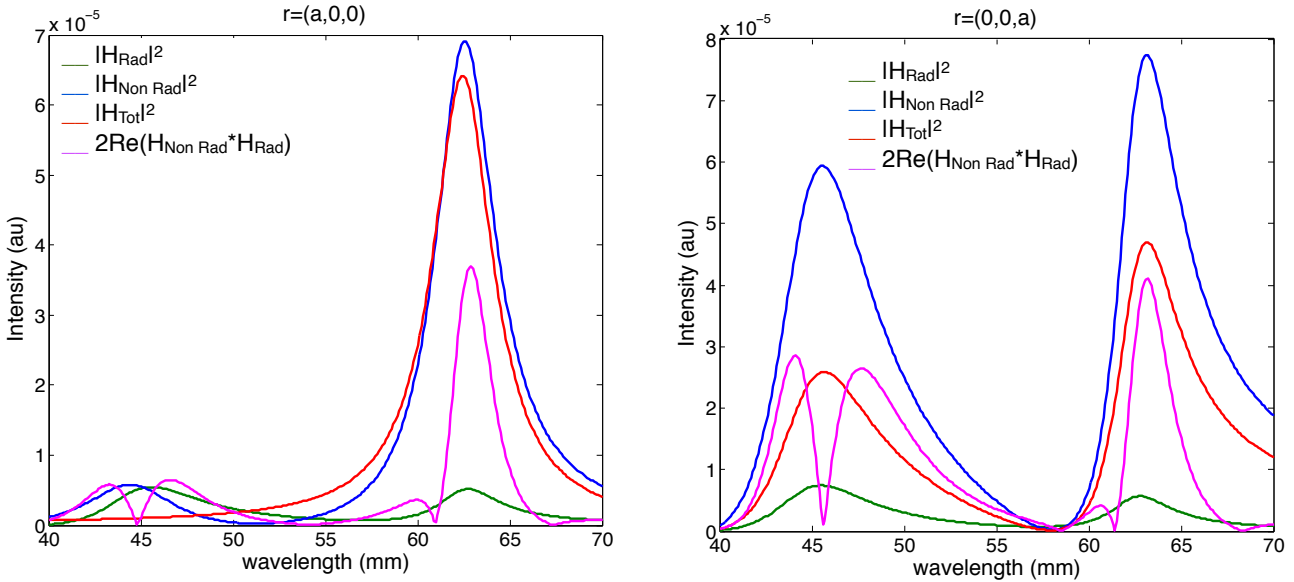


Figure 4.16. Spectral evolution of the radiative (green line), non radiative (blue line) contribution as well as their interference (magenta line) to the magnetic scattered field. The total magnetic scattered field is represented by the red solid line. All the contributions have been calculated in the points $r=(a,0,0)$ (left), and $r=(0,0,a)$ (right).

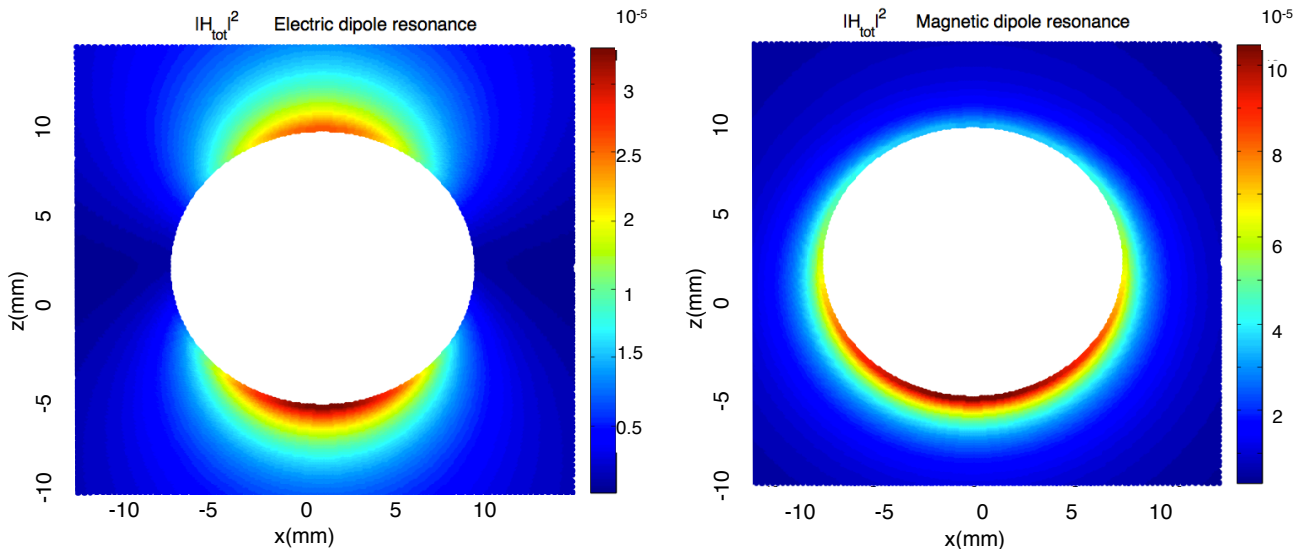


Figure 4.17. Intensity of the magnetic field scattered by an HRI spherical particle of radius $a=7.5\text{mm}$ and refractive index $n=4$. The excitation wavelength is $\lambda \approx 47\text{ mm}$ (left) and $\lambda \approx 63\text{ mm}$ (right). This wavelength corresponds with the electric dipole excitation wavelength (left) and the magnetic dipole excitation wavelength (right).

Some interesting features can be observed in *figure 4.16* and *4.17* concerning the distribution of the total scattered field and the intensity of its contributions.

First, *figure 4.16* shows how two resonance peaks appear in the spectrum. The first one, produced at $\lambda \approx 47 \text{ mm}$, is caused by the electric dipolar term of the dipole approximation, and the other one, $\lambda \approx 63 \text{ mm}$, by the magnetic dipolar term. However, the intensity of the scattered magnetic field is much smaller, five orders of magnitude, than the intensity of the electric scattered field (see *figure 4.10*).

Another important thing can be seen in *figure 4.16*. The non radiative contribution dominates over the radiative contribution. However, the latter is not negligible as in the case of metallic nanoparticles. Once again, the interference between both contribution is not negligible. Furthermore, the interference in some situations takes values comparable to the intensity of the total magnetic field.

The intensity values of the resonance peaks are in accordance with the results of the intensity maps in near field showed in *figure 4.17*. In addition, it can be seen how the back scattered magnetic field is more intense than the one scattered in the forward direction. In fact, for a wavelength $\lambda \approx 58 \text{ mm}$ the intensity of the magnetic field scattered at the point $(a, 0, 0)$ is equal to zero. This special situation is one of the Kerker's condition (see section 3.6). More precisely this corresponds to the zero forward condition.

By decomposing the scattered field into the electric and the magnetic dipolar terms, it is possible to see how the total and the non radiative contributions are red shifted with respect to the radiative contribution (*Figure 4.18* and *Figure 4.19*). Once again, due to the fact that the radiative contribution dominates over the non radiative contribution in the far field regime, the evanescent waves can be responsible for this red shift .

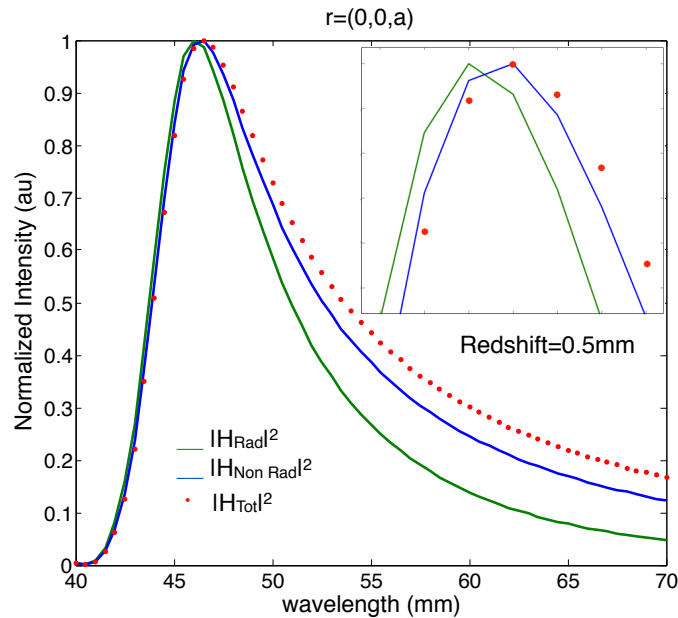


Figure 4.18. Normalized spectral evolution of the magnetic scattered field (red dots) and its radiative (green solid line) and non radiative contribution (blue solid line). The magnetic field is considered to be scattered by the electric dipolar term of the dipole approximation for an HRI with radius $a=7.5 \text{ mm}$ and $\epsilon=16$ at the point $(0,0,a)$.

In far field, where the radiative contribution dominates, the peaks are narrower than in near field (see *Figure 4.9*). Due to the fact that in near field the non radiative contribution is also broader than the radiative contribution and it dominates over the latter, the evanescent waves are also responsible for the broadening.

The red shift in the case of the magnetic scattered field by the magnetic dipolar term, (figure 4.19) is much smaller than in the case of the electric dipolar term. In addition, the broadening of the peaks is negligible.

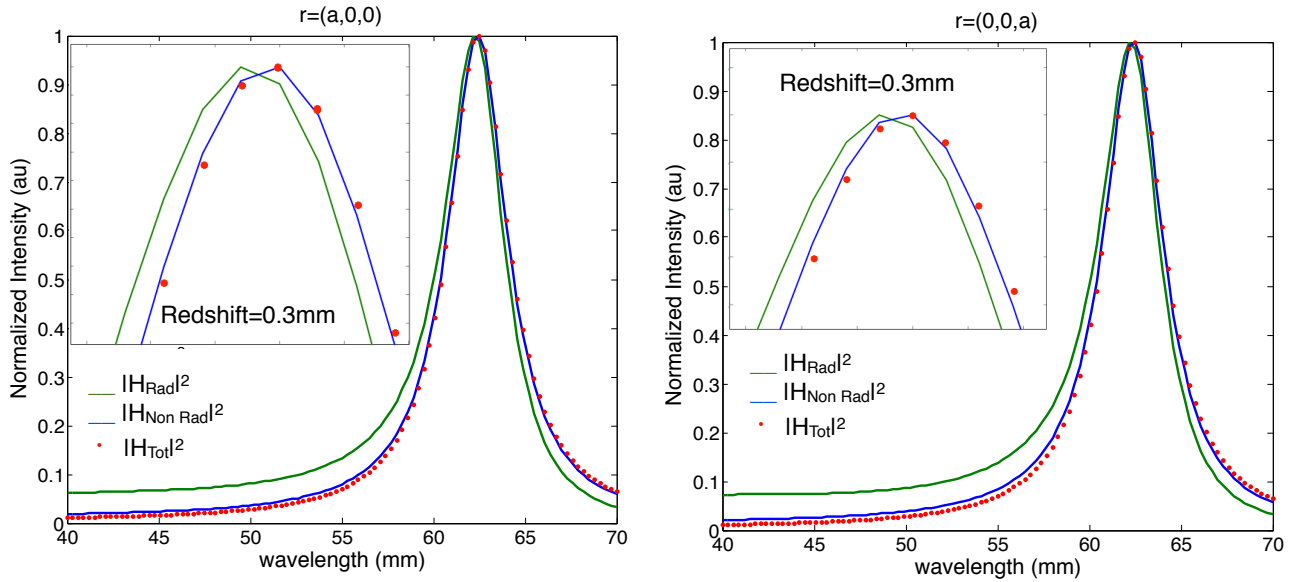


Figure 4.19. Normalized spectral evolution of the magnetic scattered field intensity (red dots) and its radiative (green solid line) and non radiative contribution (blue solid line). The magnetic field is considered to be scattered by the magnetic dipolar term of the dipole approximation for an HRI with radius $a=7.5$ mm and $\epsilon=16$. The calculus has been done in two different points: $(a,0,0)$ (left) and $(0,0,a)$ (right).

Although for the electric dipolar term (figure 4.18) the non radiative contribution does not exactly matches the total scattered field, in the case of the magnetic dipolar term (figure 4.19) they are nearly equal. The discrepancy between the non radiative and the total scattered fields can be produced by the interference between the radiative and non radiative contribution. This term, that was negligible for metals, it is not for HRI particles.

Once again, a more general analysis will be done by normalizing to the Mie scattering coefficients: a_1 in the case of the electric dipolar term and b_1 for the magnetic dipolar term of the dipole approximation.

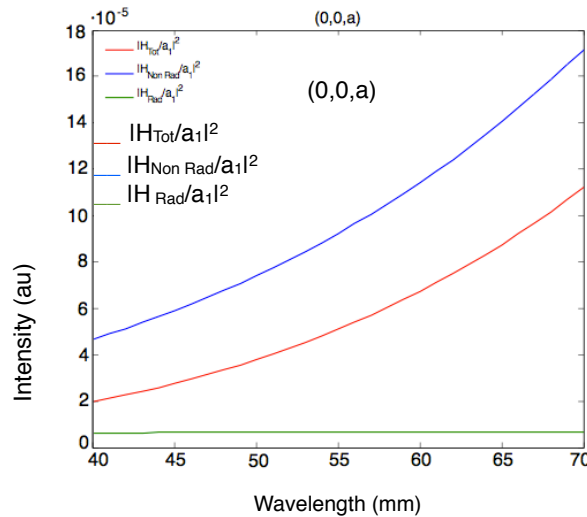


Figure 4.20. Spectral evolution of $|H_{Tot}/a_1|^2$ (red line), $|H_{non rad}/a_1|^2$ (blue line) and $|H_{rad}/a_1|^2$ (green line) at $(0,0,a)$.

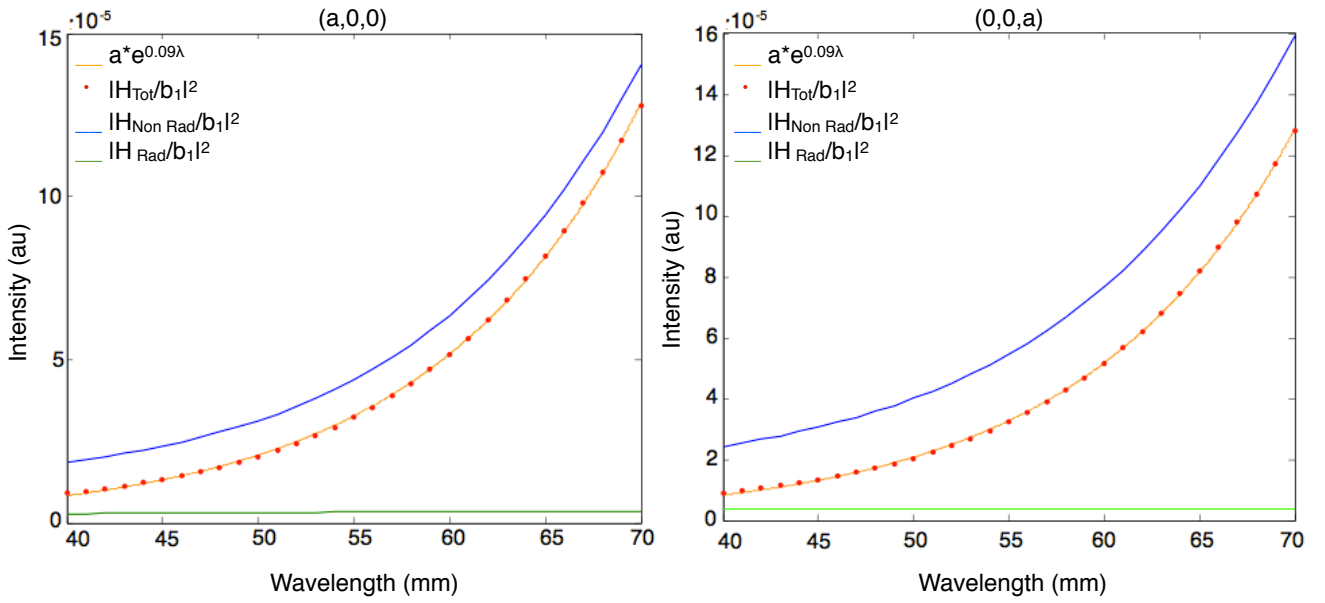


Figure 4.21. Spectral evolution of $|H_{\text{Tot}}/b_1|^2$ (red line), $|H_{\text{non rad}}/b_1|^2$ (blue line) and $|H_{\text{rad}}/b_1|^2$ (green line) at two positions, $(a,0,0)$ (left) and $(0,0,a)$ (right). The orange line represents the numeral fitting of the spectral evolution of the total field to a function $a \cdot e^{0.09\lambda}$.

Figure 4.20 and figure 4.21 shows two important features. First, in near field, the non radiative contribution dominates over the radiative one. This can be seen by comparing the blue dots with the green solid line. However, the total scattered field do not matches the non radiative contribution. This difference can be caused by the interference between the radiative and non radiative contribution.

Second, by the numerical fitting, it can be seen how the total magnetic field scattered by the magnetic dipole, shows an universal dependence with the wavelength. At both points it scales to a exponential law $a \cdot e^{0.09\lambda}$. This is different from the far field behavior, where the total scattered field follows a power law $a + b\lambda^n$ with $n \approx 2$.

4.4.5 SPECTRAL EVOLUTION OF THE POYNTING VECTOR OF THE ELECTROMAGNETIC SCATTERED FIELD BY HIGH REFRACTIVE INDEX NANOPARTICLES IN FIELD IN NEAR AND FAR FIELD.

The next plots show the modulus of the Poynting vector, $|S|$, of the scattered electromagnetic field by the electric and magnetic dipole as function of the wavelength at the electric and magnetic dipole resonances in near and far field.

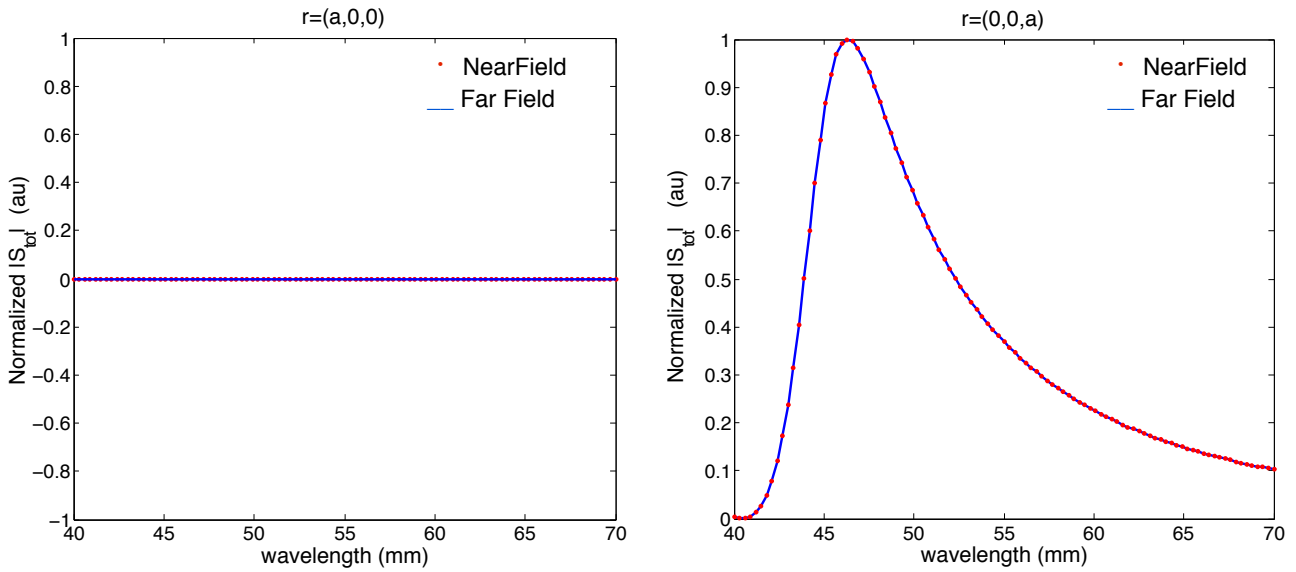


Figure 4.22. Spectral evolution of the Poynting vector of the electromagnetic scattered field by the electric dipole at the points $(a,0,0)$ (left) and $(0,0,a)$ (right) in near (red dots) and far (blue solid line) field. For the calculus an HRI nanoparticle with $a=7.5$ mm and $\epsilon=16$ has been considered.

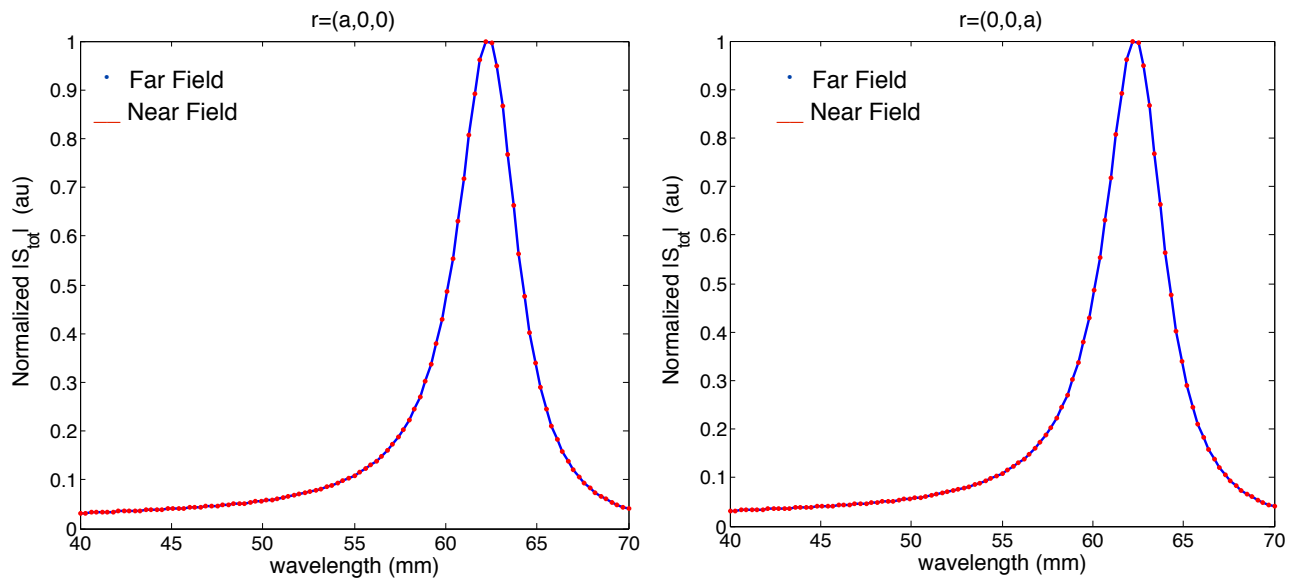


Figure 4.23. Spectral evolution of the Poynting vector of the electromagnetic scattered field by the magnetic dipole at the points $(a,0,0)$ (left) and $(0,0,a)$ (right) in near (red dots) and far (blue solid line) field. For the calculus an HRI nanoparticle with $a=7.5$ mm and $\epsilon=16$ has been considered.

Although the peaks of the electric and magnetic scattered fields at the electric and magnetic dipole resonances are red shifted and widened in near field with respect to the far field regime (see sections 4.4.1 and 4.4.2), the intensity of the electromagnetic field, modulus of the Poynting vector, shows exactly the same behavior at the electric and magnetic dipole resonances in near and far field.

4.4.6 RADIATIVE AND NON RADIATIVE CONTRIBUTION TO THE POYNTING VECTOR OF THE ELECTROMAGNETIC FIELD SCATTERED BY HIGH REFRACTIVE INDEX NANOPARTICLES IN NEAR FIELD.

In this section we will discuss the radiative and non radiative contribution to the total Poynting vector in the near field regime. The modulus of this magnitude, $|S|$, represents the energy flux associated to the electromagnetic radiation. Although in far field $|S|=|E|^2$, in near field this identity is not valid. In near field it is necessary to use its definition: $|S|=1/2|E \times H|$.

In the next figures, a specific case of an HRI index particle of $\epsilon=16$ is studied. The spectral evolution of the Poynting vector of the electromagnetic scattered field, $|S|$, its radiative and non radiative contribution has been calculated at two different points, $(a,0,0)$ and $(0,0,a)$, and for a range of wavelengths between the 40 and 70 mm.

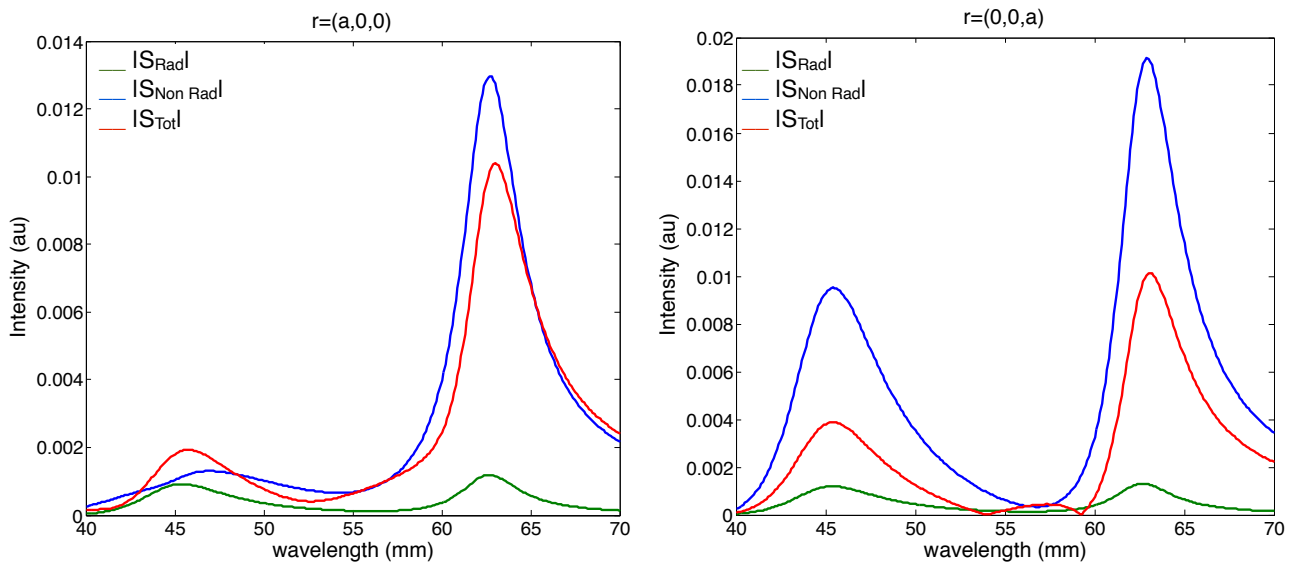


Figure 4.24. Spectral evolution of the radiative (green line), non radiative (blue line) to the Poynting vector (red line) of the electromagnetic field scattered by an HRI nanoparticle with radius $a=7.5$ mm and $\epsilon=16$. All the contributions have been calculated in the points $r=(a,0,0)$ (left), and $r=(0,0,a)$ (right).

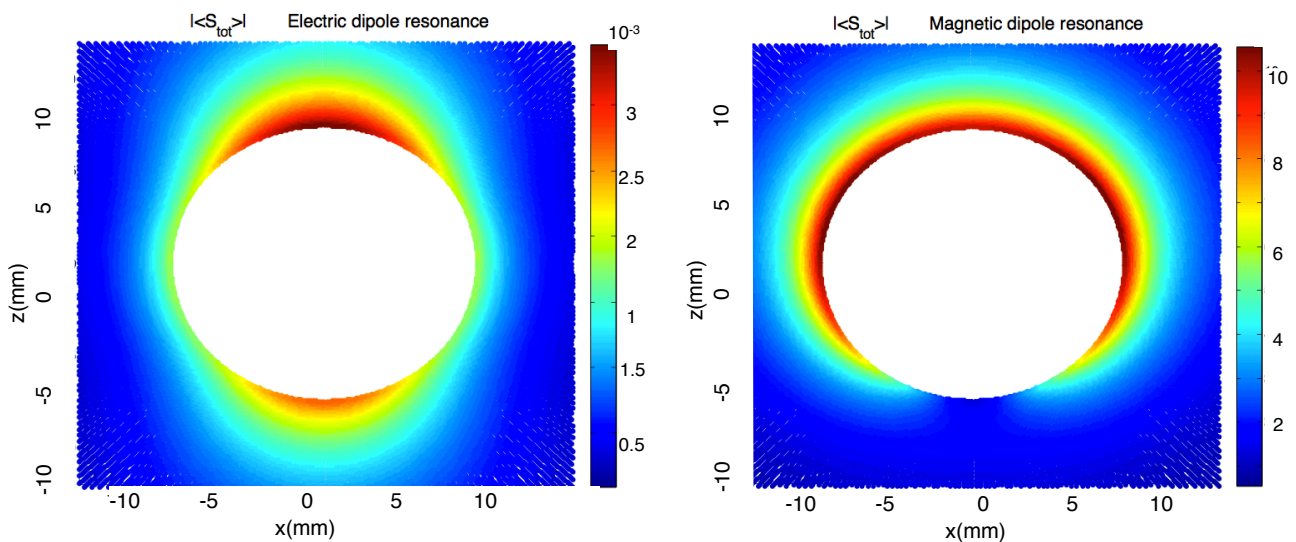


Figure 4.25. Intensity of the electromagnetic field scattered, $|S_{tot}|^2$ by an HRI spherical particle of radius $a=7.5$ mm and refractive index $\epsilon=16$. The excitation wavelength is $\lambda \approx 47$ mm (left) and $\lambda \approx 63$ mm (right). This wavelength corresponds with the electric dipole excitation wavelength (left) and the magnetic dipole excitation wavelength (right).

Once again, as it was expected, since HRI nanoparticles have been studied, the electric and magnetic dipole resonances can be seen (see *Figure 4.24*). At both resonances the non radiative dominates over the radiative contribution.

By decomposing the scattered field into the electric and the magnetic dipolar terms in the dipole approximation, it is possible to see how the total and the non radiative contributions are red shifted with respect to the radiative contribution (*Figure 4.26* and *Figure 4.27*). However, for the Poynting vector, no red shift and broadening can be seen in near field with respect to far field (*Figure 4.22* and *Figure 4.23*).

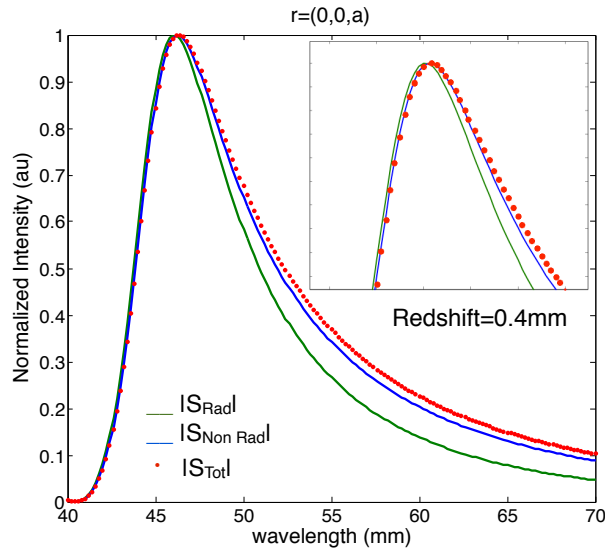


Figure 4.26. Normalized spectral evolution of the intensity of the electromagnetic scattered field (red dots) and its radiative (green solid line) and non radiative contribution (blue solid line). The electromagnetic field is considered to be scattered by the electric dipolar term of the dipole approximation for an HRI with radius $a=7.5$ mm and $\epsilon=16$ at the point $(0,0,a)$.

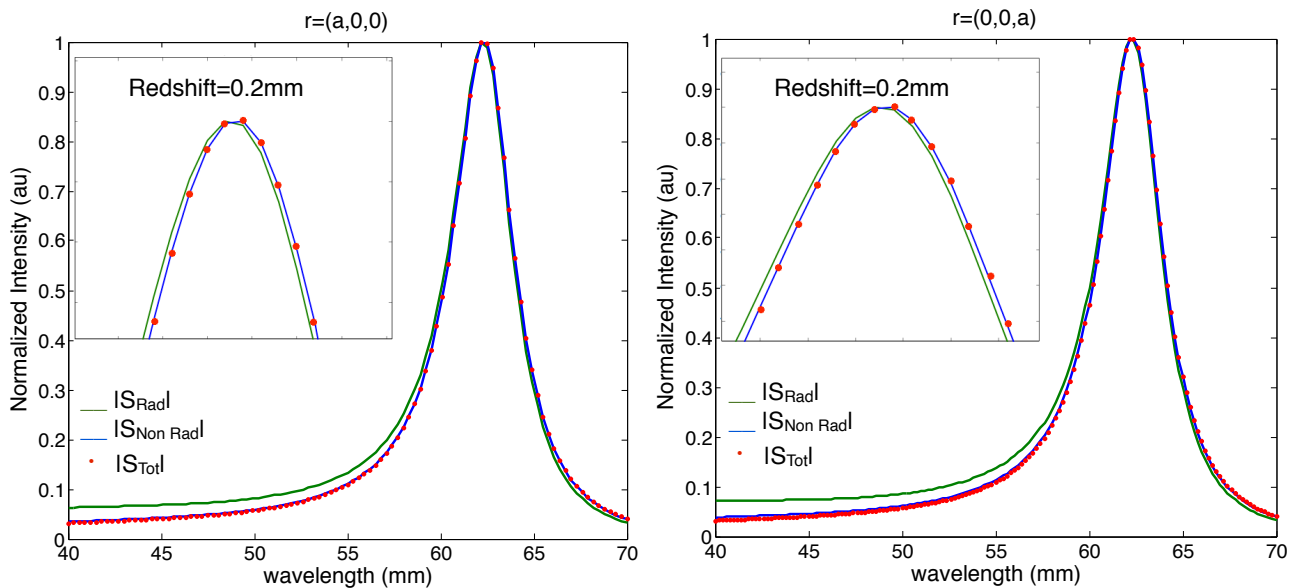


Figure 4.27. Normalized spectral evolution of the intensity of the electromagnetic scattered field (red dots), its radiative (green solid line), and non radiative contribution (blue solid line). The electromagnetic field is considered to be scattered by the magnetic dipolar term of the dipole approximation for an HRI with radius $a=7.5$ mm and $\epsilon=16$. The calculus has been done in two different points: $(a,0,0)$ (left) and $(0,0,a)$ (right).

The red shift and broadening of the non radiative contribution with respect to the radiative contribution has no effect on the behavior on near field with respect to far field because the Poynting vector represents the flux associated to the electromagnetic radiation. The non radiative contribution keeps attached to the surface of the nanoparticle and does not contribute to the flux of the electromagnetic radiation. As a result, only the radiative contribution takes part on the Poynting vector in both, far and near field regimens, and no red shift and broadening are observed.

5. CONCLUSIONS

An study of the scattered field by both metallic and high refractive index nanoparticles in the near field and far field has been done. The scattered field has been studied by means of its spectral evolution. In order to give an explanation to the differences observed, the radiative and non radiative contribution of the scattered field in far and near field has been calculated.

Although the exact solution of the scattered field by a spherical nanoparticle with arbitrary size and electric permittivity is given by Mie Theory, for HRI and metallic spherical nanoparticles with a size smaller than the wavelength of the incident electromagnetic field, it is possible to use the dipole approximation. It has been proved how the results obtained by means of the dipole approximation exactly matches the results given by Mie theory. As a result, the dipole approximation is a good approach to the study of metallic and HRI nanoparticles.

By representing the spectral evolution of the Poynting vector and the total electric and magnetic field scattered by the electric and magnetic dipole terms of the dipole approximation for HRI nanoparticles in near and far field it is observed that:

- The resonance peak of the electric and magnetic field scattered by the electric dipolar term in near field is red shifted and widened with respect to the peak in far field.
- The resonance peak of the electric and magnetic field scattered by the magnetic dipolar term in near field is red shifted but hardly widened with respect to the peak in far field.
- In the case of the Poynting vector calculated from the electric and magnetic scattered fields, it shows the same behavior in near and far field for both dipolar terms of the dipole approximation.

By the study of the radiative and non radiative contribution to the Poynting vector and the electric and magnetic field in near field it is observed that:

- The non radiative contribution in near field dominates over the radiative contribution unlike in the far field regime. However, the latter is not negligible as in the case of metallic particles in near field.
- The interference between the radiative and non radiative contribution is not negligible too.
- The non radiative contribution to the resonance peak of Poynting vector and the electric and magnetic field by the electric dipolar term is red shifted and widened with respect to the radiative contribution.
- The non radiative contribution to the resonance peak of Poynting vector and of the electric and magnetic field by the magnetic dipolar term is red shifted and hardly widened with respect to the radiative contribution.
- The non radiative contribution has a very similar behavior to the total scattered field in near field. The differences may be caused by the interference term.

Therefore, the non radiative contribution, which dominates over the radiative contribution in near field, may be responsible of the red shift and broadening of the resonance peaks in near field with respect to far field.

In the case of the Poynting vector the red shift between contributions does not lead to a difference of behavior on near field with respect to far field. The Poynting vector measures the flux of electromagnetic radiation. Because the fact that the non radiative contribution keeps attached to the surface of the scatterer, it has not effect on the electromagnetic flux. As a result, the non radiative contribution has not any effect on the Poynting vector and no red shift or broadening can be observed.

6. FURTHER WORK

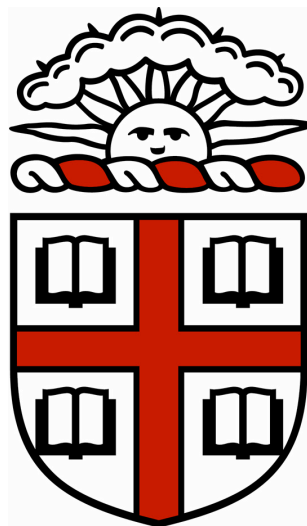
It may be interesting to extend the present work by study and analyzing the following topics:

- The effect on the radiative and non radiative contribution of placing HRI nanoparticles in a dielectric medium with $\epsilon \neq 1$.
- The effect on the radiative and non radiative contribution of considering HRI nanoparticles with a electric permittivity with an imaginary part different from zero, $\epsilon_i \neq 0$.
- The effect on the radiative and on radiative contribution when some impurities are introduced into the HRI nanoparticle.
- To introduce in the calculus the electric and magnetic quadrupolar terms.

7. BIBLIOGRAPHY

- [1] Mark I. Stockam, *Nanoplasmonics: The physics behind applications*, American Institute of Physics, February 2011.
- [2] P. Alonso-Gonzales, P. Albella, F. Neubrech, C. Huck, J. Chen, F. Golmar, F. Casanova, L.E Hueso, A. Pucci, J. Aizpurua, R. Hillenbrand. *Experimental Verification of the Spectral Shift between Near- and Far-Field Peak Intensities of Plasmonic Infrared Nanoantennas*. Phys. Rev. Lett. 2013, 110, 203902
- [3] J. Zuloaga, P. Nordlander. *On the shift between Near-Field and Far-Field peak intensities in localized plasmon system*. NonoLett.11, 1280 (2011).
- [4] Mikhail A. Kats, Nanfang Yu, Patrice Genevet, Zeno Gaburro and Federico Capasso. *Effect of radiation damping on the spectral response of plasmonic components*. Optics Express, Vol. 19, Issue 22, pp. 21748-21753 (2011)
- [5] C. Menzel, E. Hebestreit, S. Mühlig, C. Rocksstuhl, S. Burger, F. Lederer, T. Pertsch, *The spectral shift between near- and far-field resonances of optical nano-antennas*, 2014, Optical Society of America, Vol.22, No.8.
- [6] F. Moreno, P. Albella and M. Nieto-Vesperinas, *Analysis of the Spectral Behaviour of Localized Plasmon Resonances in the Near- and Far- Field Regimes*, Langmuir 2013, 29, 6715-6721.
- [7] M. Gomilšek, *Whispering gallery modes*, University of Ljubljana, November 2011.
- [8] Craig F. Bohren, Donald R. Huffman, *Absorption and Scattering of Light by Small Particles*, John Wiley & Sons, 1983.
- [9] George W. Mulholland, Craig F. Bohren, Kirk A. Fuller, *Light Scattering by Agglomerates: Couple Electric and Magnetic Dipole Method*, Langmuir, 1994,10.
- [10] M. Nieto-Vesperines, *Scattering and Diffraction in Physical Optics*, World Scientific Publishing, 2006.
- [11] Knut Kvien, *Angular spectrum representation of fields diffracted by spherical objects: physical properties and implementations of image field models*, J. Opt. Soc. Am. A/Vol 15, No.3, March 1998.
- [12] J.M. Geffrin, B. García-Cámara, R. Gómez-Medina, P. Albella, L.S. Froufe-Pérez, C. Eyraud, A. Litman, R. Vaillon, F. González, M. Nieto-Vesperinas, J.J. Sáenz & F. Moreno, *Magnetic and electric coherence in forward- and back-scattered electromagnetic waves by a single dielectric subwavelength sphere*. Nat. Commun. 3:1171 (2012).
- [13] M. Kerker, D.S Wang and L. Giles, *Electromagnetic Scattering by magnetic spheres*, J. Opt. Soc. Am. 73, 765-767 (1983).
- [14] Krasnok A.E., Miroshnichenko A.E., Belov P.A., Kivshar Y.S. *All-dielectric nanoantennas*. Proceedings of SPIE. Vol. 8806. pp. 880626 (2013).
- [15] Jason Valentine, Jensen Li, Thomas Zentgraf, Guy Bartal & Xiang Zhang, *An optical cloak made of dielectrics*, Nature Materials 8, 568 - 571 (2009)

ANNEX I: WORK AT BROWN UNIVERSITY



PHOTOLUMINESCENCE EXCITATION SPECTROSCOPY SET UP

June 16th - August 8th

INTRODUCTION

This work at Brown has been made through a new student exchange program between Brown and Cantabria Universities. The 8 weeks internship has been made under the supervision of Professor Rashid Zia at his lab.

The Zia Lab [1] works in the field of nanophotonics, studying light emission from solid stated quantum emitters such as atoms, quantum dots or molecules, and also developing techniques to control and enhance the light emission process by using photonic devices. Instead of using artificial scatterers as metamaterials or nanoantennas, they study their natural analogue: the multipolar transitions in solid-state quantum emitters. By studying and quantifying this transitions they can take full advantage of the light-matter interactions.

One of the latest techniques developed at Zia Lab is the Wide-Angle Energy-Momentum Spectroscopy [2]. This type of spectroscopy allows to measure simultaneously the spectral distribution and the momentum of light emission while maximizing the collected signal.

At Zia Lab, the tasks assigned to me were:

- Learn how to operate the white light source Energetiq EQ 1500 LDLS.
- Alignment of a parabolic mirror system with and without shearing plate interferometer.
- Build a photoluminescence excitation spectroscopy set up with an inverted microscope system.

The main objective of my work at Brown, the performance of the essential parts in the experimental set up, and all the built set ups are explained in the next sections.

OBJECTIVES AND ESSENTIAL COMPONENTS FOR THE SET UP

The main objective of the work developed at Brown University was to build an experimental set up to do photoluminescence excitation (PLE) spectroscopy by using a white light source.

In PLE spectroscopy the light emission of a sample is measured for a fixed wavelength while the excitation wavelength is varied. Therefore, for this kind of spectroscopy it is necessary to illuminate the sample with a wide range of wavelengths. In this case, a white light source and a diffraction grating to separate each wavelength has been used to achieve this goal.

The light source available for doing this set up was a broadband laser-driven light source [3]. In this kind of lamps, light is produced in a very particular way: a very powerful laser beam is focused into a Xenon plasma in order to heat it. When the temperature is high enough, light is emitted.

The advantage of this type of lamps is that they emit a very broad spectrum, from ultraviolet (UV) to the near-infrared (NIR), and it is possible to obtain very bright light no matter the wavelength. In the next figure is shown the spectral radiance versus the wavelength of the light emitted by the lamp used for this work, a Energetiq EQ 1500 LDLS:

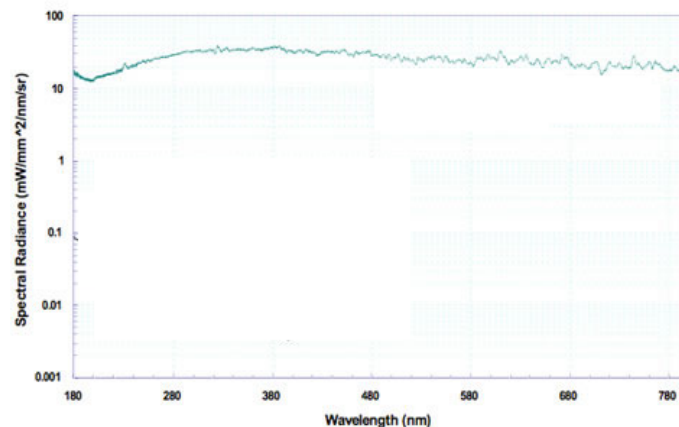


Figure 5. Spectral radiance versus the wavelength of the light emitted by the lamp Energetiq EQ 1500 LDLS [3].

In order to collimate the light coming from the light source, off-axis parabolic (OAP) mirrors [4] were used. This type of mirrors were chosen because they are able to create a collimated beam from point sources. This means that they convert spherical into planar wavefronts and vice versa.

However, the alignment of these systems that use more than one OAP mirrors is very complex. There are four essential parameters in order to achieve a good alignment: distance, angle between the OAP and the beam, the tip and the tilt. The last two parameters are easy to vary if the OAP mirrors are placed in proper mounts that have knobs to do this type of movements.

When a system like this is going to be aligned, a shearing interferometer [5] can be used. This device makes easier the process of alignment because the shape of the interference pattern indicates which parameter should be modified.

For collimation, the previous four parameters are important. When the fringes are tilted, the beam is converging or diverging, so the point source is not at the focus of the OAP (*see figure 6*). As a result, the distance between the source and the mirror should be changed. However, if the fringes are not straight, the angle between mirror and beam, the tip and the tilt should be varied.

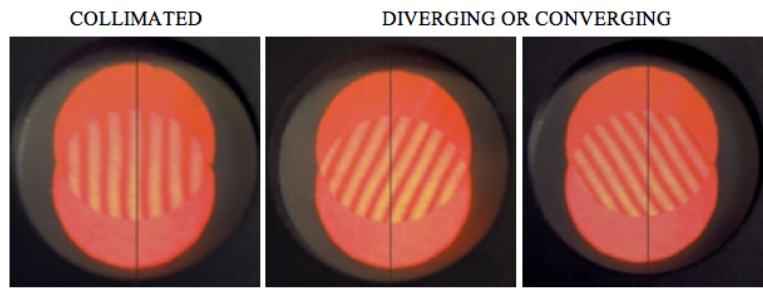


Figure 6. Image at the shearing interferometer when it is used to collimated a beam using an off-axis parabolic mirror. When the fringes are straight the beam is collimated. However, when the fringes are tilted, the beam is diverging or converging, and the position of the mirror should be changed [5].

For focusing a collimated beam, only the angle between the OAP and the collimated beam is important.

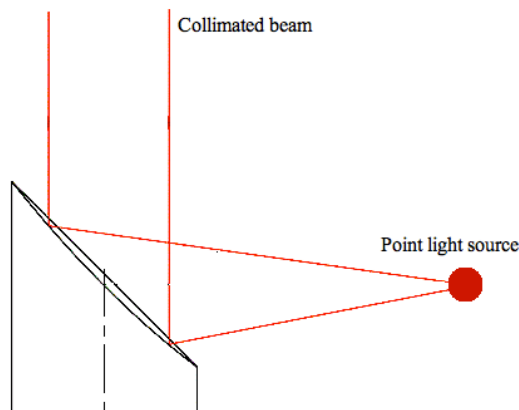


Figure 7. Scheme of a off axis parabolic mirror. The light coming from a point light source with a spherical wavefront is collimated (planar wavefront) in the reflection with the mirror. The reversed process is also possible.

The problem with the alignment of these systems is that the interferometer bases its performance on the interference of the beam. The interference phenomena needs the coherence, both temporal and spatial, of the light. When the light source is a laser the interferometer works perfectly, however, when a white light source is used, the interference pattern is not observed because the beam is not coherent. In order to improve the coherence of the white light beam, and be able to use the interferometer, several things were tried. First, a filter was placed at the output of the source in order to select only one wavelength. Then a pinhole was placed before the filter. It was not possible to see an interference pattern in any of the previous cases.

A possible solution to this problem was to do the alignment with a laser and then replace it with the white light source. However, there was not enough time to try this, so the alignment was made without the use of the shearing plate interferometer.

EXPERIMENTAL SET UPS

In order to do PLE spectroscopy several set ups were tried. However, none of them seem to be able to obtain an extinction spectrum from a thin film sample doped with Eu^{3+} .

The first experimental set up that was tried is shown in *figure 8*. In this set up the light from the source is collimated by using an off axis parabolic mirror (OAP). Then, the beam hits a diffraction grating that allows us to select the excitation wavelength by changing the angle between the beam and the grating. Afterwards, the light hits two OAPs, and the collimated beam that results from these two reflections is redirected to a microscope objective (MO) that focus the light into the sample. The light emitted by the sample goes through another MO that produces the collimation of the beam and sends it to a spectrograph. In the spectrograph, the intensity of the light is measured for a wavelength fixed by means of a computer.

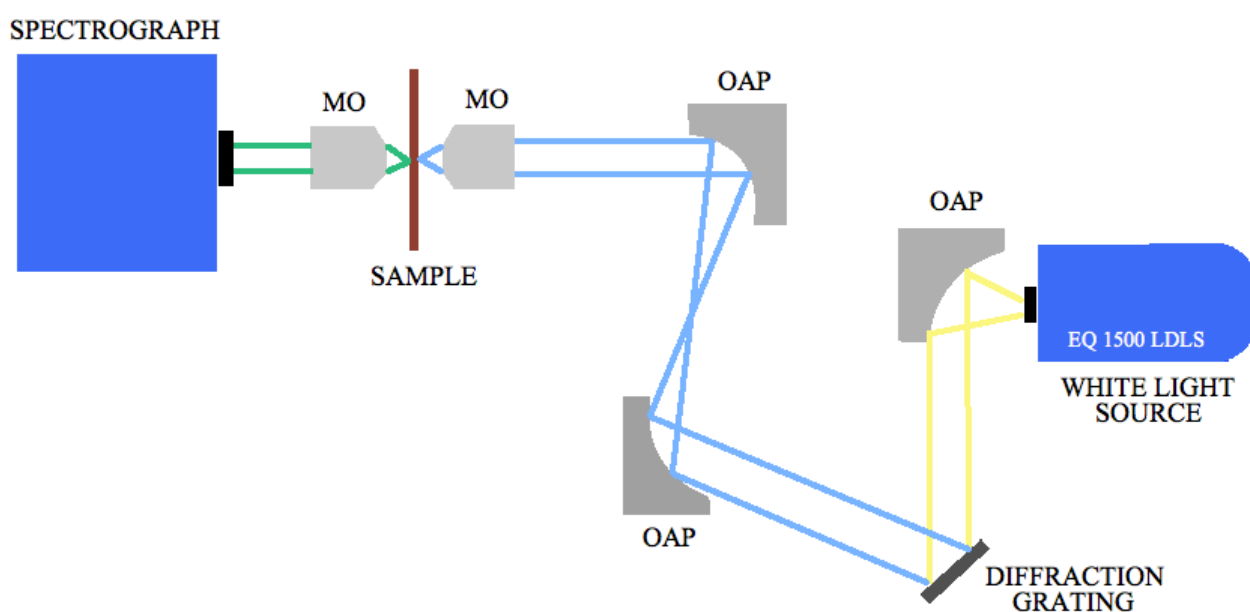


Figure 8. Photoluminescence excitation spectroscopy setup. OAP: Off axis parabolic mirror. MO: Microscope objective.

Because we were not able to obtain an extinction signal from the sample (thin film doped with Eu^{3+}),⁴⁹⁴⁷⁴⁷ another experimental set up was tried (see *figure 9*). In this case, instead of using two MO, only one was used followed by a dichroic mirror (DM) [6]. This kind of mirror lets some wavelengths to pass through it and reflects others. So the light from the OAPs its redirected to the MO that focus the light into the sample. The emitted light, which has a bigger wavelength than the excitation light, goes through the MO and is reflected by the DM to the spectrograph. Neither this way we were able to obtain a signal.

One of the possible improvements to this previous set up was to reduce the spot size at the back of the MO. Because the size of the spot was bigger than the back of the MO, a lot of light intensity was lost. In order to decrease the spot size, a spatial filter was placed before the MO (see *figure 10*). However, even with this improvement, we were not able to obtain the excitation signal.

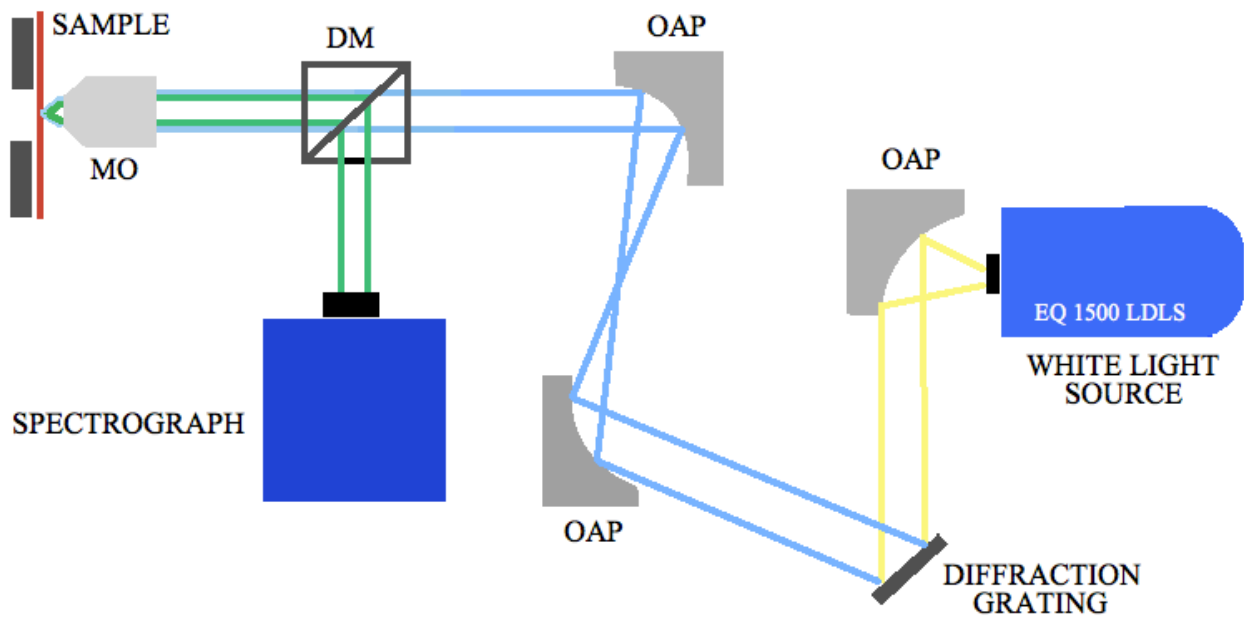


Figure 9. Photoluminescence excitation spectroscopy setup. OAP: Off axis parabolic mirror. MO: Microscope objective. DM: dichroic mirror.

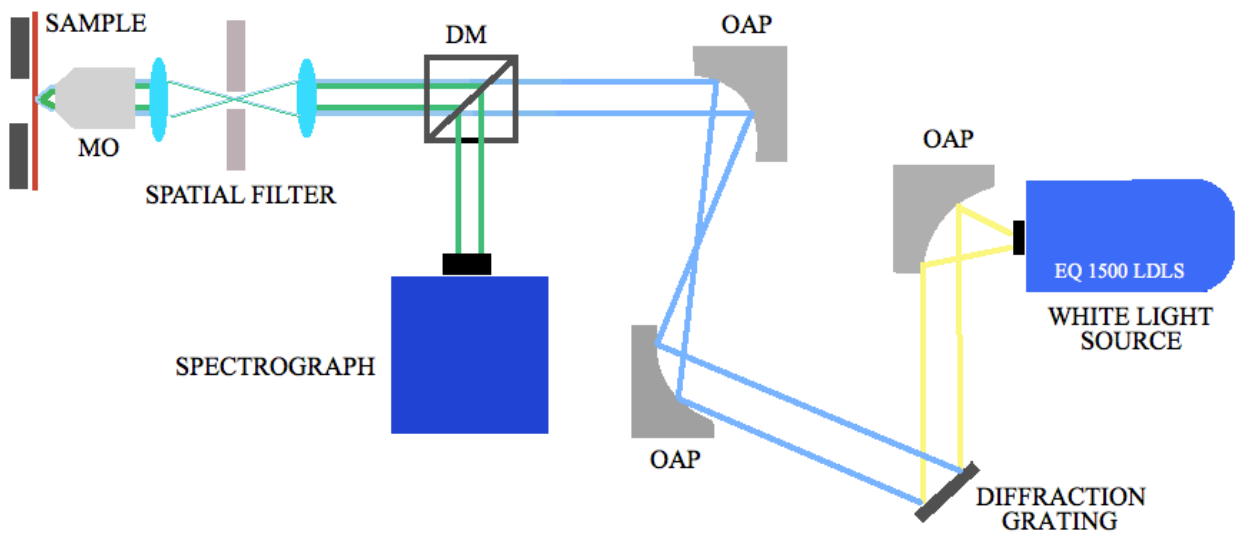


Figure 10. Photoluminescence excitation spectroscopy setup. OAP: Off axis parabolic mirror. MO: Microscope objective. DM: dichroic mirror.

BIBLIOGRAPHY

[1] Zia Lab website: www.zia-lab.com/

[2] C. M. Dodson, Kurvits, J. A., Li, D., and Zia, R., “Wide-Angle Energy-Momentum Spectroscopy”, *Opt. Lett.*, vol. 39, pp. 3927–3930, 2014.

[3] Energetiq EQ1500 LDLS daa sheet: www.energetiq.com/DataSheets/EQ1500_Data_Sheet_.pdf

[4] Off-axis parabolic mirrors, Thorlabs: http://www.thorlabs.de/newgrouppage9.cfm?objectgroup_id=7002

[5] Shearing interferometers, Thorlabs: http://www.thorlabs.de/newgrouppage9.cfm?objectgroup_id=2970